






Latitudinal constraints on the abundance and activity of the cyanobacterium UCYN-A and other marine diazotrophs in the North Pacific

Mary R. Gradoville ^{1,*} Hanna Farnelid,^{1,a} Angelicque E. White ² Kendra A. Turk-Kubo,¹ Brittany Stewart,^{1,b} François Ribalet ³ Sara Ferrón ² Paulina Pinedo-Gonzalez,^{4,c} E. Virginia Armbrust,³ David M. Karl ² Seth John,⁴ Jonathan P. Zehr¹

¹Ocean Sciences Department, University of California Santa Cruz, Santa Cruz, California

²Department of Oceanography, University of Hawaii at Manoa, Honolulu, Hawaii

³School of Oceanography, University of Washington, Seattle, Washington

⁴University of Southern California, Los Angeles, California

Abstract

The number of marine environments known to harbor dinitrogen (N₂)-fixing (diazotrophic) microorganisms is increasing, prompting a reassessment of the biogeography of marine diazotrophs and N₂ fixation rates (NFRs). Here, we investigate the diversity, abundance, and activity of diazotrophic microorganisms in the North Pacific Subtropical Gyre (NPSG), a diazotrophic habitat, and the North Pacific Transition Zone (NPTZ), a region characterized by strong physical, chemical, and biological gradients. Samples were collected on two springtime meridional cruises during 2016 and 2017, spanning from 23.5°N to 41.4°N along 158°W. We observed an abrupt decrease in diazotrophic abundances near the southern edge of the NPTZ, which coincided with a salinity front and with a ~10-fold increase in *Synechococcus* abundance, but without a concomitant change in phosphate or nitrate concentrations. In NPSG waters south of this diazotrophic boundary, *nifH* genes and NFRs were consistently detected and diazotrophic communities were dominated by UCYN-A, an uncultivated, symbiotic cyanobacterium (2.8×10^3 to 1.0×10^6 *nifH* gene copies L⁻¹). There was a significant positive relationship between quantitative polymerase chain reaction-derived UCYN-A *nifH* gene abundances and community NFRs in the NPSG, suggesting a large contribution of UCYN-A to community NFRs. In the NPTZ waters to the north, NFRs were low or undetected and *nifH* genes were rare, with the few detected sequences represented by UCYN-A and noncyanobacterial diazotrophs. The patterns we observed in UCYN-A abundance in the context of local biogeochemistry suggest that the environmental controls of this organism may differ from those of cultivated marine cyanobacterial diazotrophs.

The biological reduction of dinitrogen (N₂) gas to ammonia (N₂ fixation) provides nearly half of the planet's bioavailable nitrogen (N) (Galloway et al. 2004) and can fuel a large fraction of productivity and export in N-limited ocean ecosystems (Karl

et al. 1997). The process of N₂ fixation is performed by a select group of microorganisms, termed diazotrophs, that possess the enzyme nitrogenase. For the past half century, marine N₂ fixation has been thought to be primarily restricted to surface waters of the tropical and subtropical oceans, where N-limitation can select for diazotrophs (Gruber and Sarmiento 1997), cyanobacterial diazotrophs can photosynthesize, and temperatures are warm enough to facilitate the growth of the well-known diazotrophic cyanobacterium, *Trichodesmium* (Breitbart et al. 2007). However, sequencing of the nitrogenase (*nifH*) gene has revealed unicellular cyanobacterial and diverse non-cyanobacterial marine diazotrophs with broad geographic ranges (Zehr et al. 1998; Moisaner et al. 2010; Farnelid et al. 2011). Furthermore, recent surveys have reported diazotrophic genes and/or N₂ fixation rates (NFRs) in unexpected environments, including high-nutrient coastal systems (Mulholland et al. 2012; Bentzon-Tilia et al. 2015), oxygen minimum zones

*Correspondence: mgradovi@ucsc.edu

This is an open access article under the terms of the Creative Commons Attribution License, which permits use, distribution and reproduction in any medium, provided the original work is properly cited.

Additional Supporting Information may be found in the online version of this article.

^aPresent address: Hanna Farnelid, Centre of Ecology and Evolution in Microbial Model Systems, Linnaeus University, Kalmar, Sweden

^bBrittany Stewart, University of Southern California, Los Angeles, California

^cPaulina Pinedo-Gonzalez, Lamont-Doherty Earth Observatory, Columbia University, New York, New York

(Loescher et al. 2014; Jayakumar et al. 2017), polar regions (Blais et al. 2012; Harding et al. 2018; Shiozaki et al. 2017), and the deep sea (Hewson et al. 2007; Benavides et al. 2018). Thus, the biogeography and environmental controls of marine diazotrophs are still not well understood.

While much recent work has focused on understanding global patterns in diazotrophy, few studies have surveyed the distribution and activity of diazotrophs through the transition zones separating major biomes. These ecological transition zones are characterized by steep environmental gradients and often contain high diversity and species richness (Kark 2007). One such region is the North Pacific Transition Zone (NPTZ), which spans the Pacific basin between the North Pacific Subtropical Gyre (NPSG) and the Pacific Subarctic Gyre, comprising ~12% of the total surface area of the North Pacific. The NPTZ contains strong gradients in physical, chemical, and biological properties (Roden 1991; Polovina et al. 2001; Juranek et al. 2012). The NPTZ is bounded by thermohaline fronts: the subtropical frontal zone to the south (~32°N) is defined by a shift in surface salinity from ~35.2 to 34.8 (Roden 1991) and has been associated with surface chlorophyll blooms (Wilson 2003; Wilson et al. 2013), and the subarctic frontal zone to the north (~42°N) is defined by a shift in surface salinity from ~33.8 to 33.0 (Roden 1991) and has been associated with strong gradients in macronutrient concentrations (Park 1967; McGowan and Williams 1973). Within the NPTZ, a sharp, basin-wide gradient in surface chlorophyll termed the transition zone chlorophyll front (Polovina et al. 2017) moves seasonally ~1000 km north and south and has been associated with increased productivity and export compared to adjacent areas (Juranek et al. 2012). This chlorophyll front is likely caused by the southward Ekman transport of nutrient-rich subarctic surface waters during the winter and spring (Ayers and Lozier 2010). The multiple physical, chemical, and biological fronts within the NPTZ provide an opportunity to investigate the mechanisms that structure communities of microorganisms such as diazotrophs.

Theory, model output, and direct observations all suggest that diazotrophy should decrease through the transition from the NPSG to the NPTZ (Church et al. 2008; Ward et al. 2013). The warm surface waters of the NPSG are chronically limited in fixed N (<10 nmol nitrate L⁻¹; Karl and Church 2014) and comprise a known habitat for diazotrophs (Karl et al. 2002). Diazotrophic assemblages in the NPSG are dominated by cyanobacteria—unicellular groups (UCYN-A, *Crocospaera*, and *Cyanothece*), filamentous *Trichodesmium*, and heterocystous groups associated with diatoms—but also include putative heterotrophs (Church et al. 2005b). The abundances of these diazotrophic taxa and the magnitude of N₂ fixation-supported carbon (C) export within the NPSG vary on a seasonal cycle (Karl et al. 1997, 2012; Church et al. 2009). Further north, NPTZ waters have lower temperatures, higher inorganic N concentrations, higher nitrate:phosphate (N:P) ratios, and higher nitrate:iron (N:Fe) supply ratios, all of which have been suggested to decrease the competitive ability of diazotrophs

relative to other phytoplankton groups and/or inhibit N₂ fixation (Ohki et al. 1991; Stal 2009; Ward et al. 2013). A few samples collected across the NPTZ support the hypothesis that diazotrophs are rare or absent from this region (Marumo and Asaoka 1974; Church et al. 2008; Shiozaki et al. 2017). However, this area of the ocean has been extremely under-sampled for NFRs (Tang et al. 2019). Thus, the location of the boundary for diazotrophy within the NPTZ, and the biogeochemical drivers of that boundary have been largely unexplored.

The objective of this study was to determine how diazotrophic communities and NFRs vary within the NPSG and across the environmental gradients of the NPTZ. We present data from two springtime surveys from consecutive years spanning from the NPSG (~23°N) through the NPTZ and into the subarctic frontal zone (41.4°N). On both cruises, we investigated diazotrophic diversity, abundance, and activity using high-throughput sequencing and quantitative polymerase chain reaction (qPCR) of the *nifH* gene as well as ¹⁵N₂ fixation rate assays. We also used single-cell approaches to measure cell-specific NFRs by the dominant diazotroph in our samples—UCYN-A, a unique unicellular cyanobacterium living in a likely obligate symbiosis with a prymnesiophyte host (Zehr et al. 2016).

Methods

Sampling strategy and seawater collection

Samples were collected during two transect cruises in the North Pacific: a cruise aboard the *R/V Ka'imikai-O-Kanaloa*, 19 April 2016 to 3 May 2016 and a cruise aboard the *R/V Marcus G. Langseth*, 27 May 2017 to 13 June 2017 (Fig. 1).

Seawater was collected for DNA, RNA, and ¹⁵N₂ incubations using Niskin® sampling bottles attached to a rosette equipped with a conductivity, temperature, depth (CTD) and an in situ fluorometer. Seawater was sampled into 2- or 4-L acid-washed,

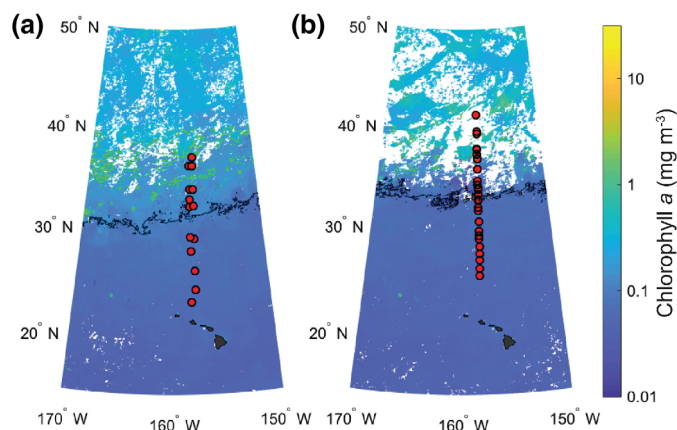


Fig. 1. Locations of sampling sites for the 2016 (a) and 2017 (b) cruises. Sites are superimposed onto sea surface chlorophyll concentrations (mg m⁻³) obtained from 4 km, 32 d-binned MODIS satellite data (<http://oceandata.sci.gsfc.nasa.gov/>) from 15 April 2016 to 16 May 2016 (a) and 17 May 2017 to 17 June 2017 (b). Black lines indicate the 18°C temperature contours.

MilliQ®-rinsed polycarbonate bottles. Samples for RNA and NFR measurements were always collected before dawn, while samples for DNA were collected at different times of day. During the 2017 cruise, additional surface (10–15 m) seawater samples for DNA were collected using the trace metal sample collection setup (see below).

During the 2016 cruise, DNA samples were sequentially filtered through 25 mm, 3 μm pore size polyethersulfone membranes (Sterlitech, Kent) then onto 0.2- μm pore size Supor membranes (Pall Corporation, New York) using a peristaltic pump. During the 2017 cruise, both DNA and RNA samples were filtered onto 0.2 μm pore size Supor membranes. DNA filtration volumes differed between the two cruises. Maximum filtration volumes were 2 L in the 2016 cruise and 4 L in the 2017 cruise, but variable biomass at the different sampling sites resulted in final filtration volumes ranging from 1050 to 2000 mL during the 2016 cruise and from 700 to 4000 mL during the 2017 cruise (see Supporting Information Table S2). RNA samples were filtered for a maximum of 25 min; filtration volumes ranged from 970–3900 mL. For both cruises, filters were placed into microcentrifuge tubes containing mixtures of 0.1- and 0.5-mm glass beads (Biospec Products, Bartlesville), 396 μL of Buffer RLT (Qiagen, Venlo, the Netherlands), and 4 μL of beta-mercaptoethanol (RNA samples) or beads only (DNA samples), then flash-frozen in liquid N_2 and stored at -80°C until analysis.

Biogeochemical and hydrological data

Surface seawater samples for nitrate plus nitrite ($\text{N} + \text{N}$) and soluble reactive phosphorus (SRP, dominated by phosphate) were collected from Niskin® sampling bottles and the ship's uncontaminated underway line into acid-cleaned high-density polyethylene bottles. The samples were immediately frozen and analyzed at the University of Hawaii following Foreman et al. (2019). Briefly, $\text{N} + \text{N}$ and SRP were measured using a SEAL Analytical AutoAnalyzer III with high-resolution detectors following the colorimetric reactions described by Strickland and Parsons (1972) and Murphy and Riley (1962), respectively. The limit of quantification for these colorimetric methods is 75 nmol L^{-1} for $\text{N} + \text{N}$ and $\sim 30 \text{ nmol L}^{-1}$ for SRP, and the average precision is 0.4% and 0.2%, respectively. Accuracies are within 2%, as determined with daily analyses of Wako CSK standard nitrate and phosphate solutions. For low $\text{N} + \text{N}$ concentrations ($< 0.5 \mu\text{mol L}^{-1}$), $\text{N} + \text{N}$ was determined using a high sensitivity chemiluminescent method, described in detail in Foreman et al. (2016), which has a detection limit of 1 nmol L^{-1} . The precision of the high-sensitivity method ranges from 0.4% at 1000 nmol L to 1–7% at 2 nmol L^{-1} .

Surface seawater samples for trace metals were collected from depths of ~ 10 –15 m while underway at speeds of 9–12 knots. The inlet tube was kept at depth using a trace metal clean surface tow fish system modified from that of Bruland et al. (2005). The water intake tube was attached to a PVC “vane” on a polypropylene line, with two PVC-encapsulated

lead-weighted “torpedoes” and roughly 50 kg of steel weights mounted below the vane. The intake tubing was connected to a deck-mounted, compressed air-powered, polytetrafluoroethylene bellows pump (AstiPure II) to pump water at a rate of 5–10 L/min. Samples were filtered in-line using 0.2 μm syringe filters (PALL Acrodisc Syringe Filter Supor Membrane).

Seawater samples were analyzed for dissolved trace metal concentrations at the University of Southern California after preconcentration using an offline adaptation of the *seaFAST*-pico metal extraction system (Elemental Scientific Inc.) as described in Lagerström et al. (2013). Briefly, using the *seaFAST*, 10 mL aliquots of seawater were extracted onto Nobias PA1 chelating resin at pH ~ 6.5 with an ammonium acetate/acetic acid buffer, then eluted in 10% vol/vol nitric acid (HNO_3). Fe concentrations were measured by isotope dilution on a Thermo Fisher Element 2 High Resolution Inductively Coupled Plasma Mass Spectrometer. The accuracy of this analytical procedure was verified by analysis of a seawater reference material (GEOTRACES GS [BATS]), for which good agreement with the reported consensus value was obtained.

Picophytoplankton groups (*Prochlorococcus*, *Synechococcus*, and picoeukaryotes) were enumerated using a continuous SeaFlow instrument (Swalwell et al. 2011). Additional discrete samples were collected alongside, fixed with glutaraldehyde (0.01% vol/vol final concentration), flash frozen, and stored at -80°C until analysis on land using an Influx flow cytometer (BD Biosciences, Seattle, WA) equipped with a 488-nm laser; emission at 692 nm (chlorophyll *a* fluorescence) and at 527 nm (phycoerythrin fluorescence) was triggered by forward light scatter. These two instruments provided comparable flow cytometric counts.

Sea surface temperature, salinity, and chlorophyll fluorescence were measured using sensors that were integrated into the CTD rosette and sensors hooked into the ship's underway uncontaminated seawater system.

Nucleic acid extraction, *nifH* amplification, and sequencing

Samples for DNA and RNA were extracted using the DNeasy and RNeasy Plant Mini Kits with the QIAcube instrument (Qiagen, Venlo, the Netherlands). DNA was extracted using the manufacturer's protocol with additional steps of three flash freeze/thaw cycles, 2 minutes of bead-beating, and Proteinase K treatment, as described by Moisaner et al. (2008). The final DNA elution volume was 100 μL . RNA was extracted according to the manufacturer's protocol, with additional steps of bead-beating and DNase treatment (RNase-Free DNase Set, Qiagen, Venlo, the Netherlands). Complimentary DNA (cDNA) was generated with the Superscript III First-Strand Synthesis System (Thermo Fisher, Waltham), using the *nifH3* gene-specific primer (Zani et al. 2000). Control reactions containing no reverse transcriptase enzyme were run for all samples to test for possible DNA contamination.

PCR was used to amplify *nifH* genes from DNA and cDNA samples using nested, degenerate *nifH* primers (Zehr and

McReynolds 1989; Zani et al. 2000). PCRs were performed using a Bio-Rad MyCycler thermocycler. The first round of PCR contained 1× Platinum *Taq* DNA polymerase PCR buffer (Thermo Fisher, Waltham), 250 μ M deoxyribonucleotide triphosphates, 4 mM MgCl_2 , 2 units Platinum *Taq* DNA polymerase (Thermo Fisher, Waltham), 0.5 μ M *nifH*3 and *nifH*4 primers, and 3 μ L DNA or cDNA, with a final reaction volume of 23 μ L. This reaction was cycled at 95°C for 3 min, followed by 25 cycles of 95°C for 30 s, 55°C for 30 s, and 72°C for 45 s, with a final extension of 72°C for 7 min. The second round of PCR had the same mixture components and thermocycling conditions (except the annealing temperature of 55°C) but included 2 μ L of PCR product from the first reaction and primers consisting of gene-specific regions (*nifH*1 and *nifH*2) and common sequence tags, as previously described (Moonsamy et al. 2013). PCRs were performed in triplicate for each sample, and products were visualized using gel electrophoresis. For samples with three successful PCRs (visual *nifH* bands), products were pooled and used for sequencing. Negative control samples (eight no-template controls and two filter blanks) were included for sequencing despite the absence of visual bands after amplification. PCR amplicons were packaged in dry ice and shipped to the DNA Services Facility at the University of Illinois at Chicago. Here, a second PCR amplification was performed to add sequencing adaptors and barcodes, then amplicons were purified, pooled, and sequenced using MiSeq Standard v.3, 2 × 300 bp paired-end sequencing according to the methods described in Gradoville et al. (2018). All raw sequence data are available from the NCBI (accession PRJNA530276).

Bioinformatic analyses

Sequence reads from partial *nifH* amplicons were de-multiplexed using the Illumina MiSeq Reporter (MSR) version 2.5.1. Paired end reads were merged using Paired-End reAd mergeR (PEAR) (Zhang et al. 2014). Merged reads were screened for quality using the screen.seqs command in mothur (Schloss et al. 2009), and sequences with ambiguities or homopolymers of ≥ 8 bp were discarded. Primers were removed using the pcr.seqs command. Singletons were removed, operational taxonomic units (OTUs) were clustered at 97% nucleotide similarity, and a de novo chimera check was performed using USearch v10 (Edgar 2010). The program Geneious v9.1.8 (www.geneious.com) was used to visualize a representative sequence from each OTU (assigned by USearch) and OTUs with representative sequences containing frameshifts, stop codons, and non-*nifH* sequences were removed. Sequences that passed these quality control steps were subsampled to 6792 sequences per sample using the single_rarefaction.py command in the Quantitative Insights Into Microbial Ecology (QIIME) bioinformatic pipeline (Caporaso et al. 2010). All negative control samples contained ≤ 70 *nifH* sequences after quality control; these samples were removed during the rarefaction step and were excluded from further analyses.

The *nifH* OTUs were translated and classified via BLAST-p similarity to a custom reference database of 879 full-length

nifH sequences derived from publicly available genomes (<https://www.zehr.pmc.ucsc.edu/Genome879/>). Taxa were binned into previously assigned *nifH* groups, with the 1B (cyanobacterial) group further classified into the groups *Trichodesmium*, *Crocospaera*, *Cyanothece*, Nostocales (*Nostoc*/*Trichormas*), and UCYN-A. The group “other” was used to bin remaining 1B OTUs, OTUs with <85% similarity to any sequence in the reference database, and OTUs with equal similarity to database sequences from different *nifH* groups.

Quantitative PCR

The *nifH* genes from nine diazotrophic taxa were enumerated using qPCR assays with Taqman® chemistry. Primer/probe sets targeted the following diazotrophic groups: *Trichodesmium* (Church et al. 2005a), *Crocospaera* (UCYN-B, Moisaner et al. 2010), *Cyanothece*-like organisms (UCYN-C, Foster et al. 2007), unicellular cyanobacterial group A1 (UCYN-A1, Church et al. 2005a), unicellular cyanobacterial groups A2 and A3 (UCYN-A2/A3, Thompson et al. 2014), *Richelia* associated with the diatom *Rhizosolenia* (Het-1, Church et al. 2005b), *Hemiaulus* associated with the diatom *Rhizosolenia* (Het-2, Foster et al. 2007), *Calothrix* associated with the diatom *Chaetoceros* (Het-3, Foster et al. 2007), and the gammaproteobacterial group “Gamma-A” (Langlois et al. 2008). All nine groups were quantified from the 2016 samples; UCYN-A1 and *Trichodesmium* were quantified from the 2017 samples.

Quantitative PCR assays were run in duplicate on an Applied Biosystems 7500 Real Time PCR System thermocycler. Details on the reaction mixtures, thermocycling conditions, preparation of standards, inhibition tests, and gene concentration calculations have been described previously (Goebel et al. 2010). The limit of detection (LOD) and limit of quantification (LOQ) for these qPCR assays have been previously determined to be 1 and 8 *nifH* copies per reaction, respectively (Goebel et al. 2010). Based on our DNA template additions (2 μ L per reaction) and filtration volumes (800–4000 mL), this corresponds to LODs ranging from 13 to 63 *nifH* copies L⁻¹ and LOQs ranging from 100 to 500 *nifH* copies L⁻¹. For 2016 samples, qPCR abundances from the two size fractions were added together to estimate total (nonfractionated) abundances.

Community NFR and carbon fixation rates

Community (bulk) C fixation rates and NFRs were measured using the ¹³C method (Hama et al. 1983; Legendre and Gosselin 1997) and the ¹⁵N₂ tracer method of Montoya et al. (1996), with modifications to avoid problems associated with incomplete bubble dissolution (Mohr et al. 2010; Chang et al. 2019). All rate measurements were conducted using surface seawater (15 m) collected from predawn CTD casts. Measurements were performed at 12 stations during the 2016 cruise (~23.5–37°N) and at 8 stations during the 2017 cruise (~25.5–36°N). During both cruises, seawater was sampled into duplicate 4.4 L acid-washed, MilliQ-rinsed polycarbonate bottles. These bottles were spiked with ¹⁵N₂ (details varied between

cruises, see below) and 1.0 mL aliquots of a 47 mM ^{13}C -labeled bicarbonate (99 atom% $\text{NaH}^{13}\text{CO}_3$, Cambridge Isotope Laboratories) using a separate, plunger-type syringe. Bottles were incubated on deck for 24 h in surface seawater-cooled incubators fitted with screening to mimic approximate in situ light conditions ($\sim 33\%$ light level). Incubations were terminated by gentle vacuum filtration onto precombusted 25-mm glass fiber filters (GF/F, Whatman). Time zero $\delta^{13}\text{C}/\delta^{15}\text{N}$ natural abundance samples were also collected from each station where $^{15}\text{N}_2$ assays were conducted; these samples were immediately filtered. Filters were frozen at -80°C and shipped to Oregon State University, where they were dried overnight at 60°C and packaged into tin and silver capsules. Particulate C, particulate N, and isotopic composition ($\delta^{13}\text{C}$, $\delta^{15}\text{N}$) were analyzed by continuous-flow isotope ratio mass spectrometry using a Carlo Erba elemental analyzer connected to a Thermo DeltaPlus isotope ratio mass spectrometer. All raw N yields were above 500 mV, which is the threshold where linearity effects are considered for this instrument.

For the 2016 cruise, the $^{15}\text{N}_2$ tracer was added as $^{15}\text{N}_2$ -enriched seawater (Mohr et al. 2010) following the procedure described by Wilson et al. (2012). Briefly, to prepare the tracer, surface seawater from Station ALOHA (A Long-term Oligotrophic Habitat Assessment, $22^\circ 45'\text{N}$, $158^\circ 00'\text{W}$) was collected approximately 1 month prior to the cruise, filtered using a $0.2\ \mu\text{m}$ in-line filter, and transported in the dark to the University of Hawaii. This seawater was degassed by bubbling with helium gas then applying vacuum pressure while heating and stirring. Next, $\sim 13\ \text{mL}$ $^{15}\text{N}_2$ gas/L of degassed seawater was added and the sample was agitated to facilitate bubble dissolution. The $^{15}\text{N}_2$ enriched seawater was transferred to glass serum bottles, which were crimp-sealed and stored at 4°C . At sea, after filling incubation bottles to capacity with collected seawater, 100–120 mL of seawater was removed and replaced with an equal volume of $^{15}\text{N}_2$ -enriched seawater. The $^{15}\text{N}/^{14}\text{N}$ ratio of the $^{15}\text{N}_2$ -enriched seawater tracer was measured via membrane inlet mass spectrometry (MIMS) according to Ferrón et al. (2016), yielding atom % $^{15}\text{N}_2$ values of $64.0 \pm 4.5\%$, $74.2 \pm 2.5\%$, $77.3 \pm 1.9\%$, and $79.7 \pm 2.7\%$ for the four batches of $^{15}\text{N}_2$ -enriched seawater we produced. These values were used to calculate the initial atom % $^{15}\text{N}_2$ of incubation bottles. Measuring the $^{15}\text{N}/^{14}\text{N}$ ratio in the $^{15}\text{N}_2$ -enriched seawater instead of in the final sample may have been a source of error for the 2016 incubations (White et al. 2020).

For the 2017 cruise, in order to reduce the potential addition of nutrients from $^{15}\text{N}_2$ -enriched seawater (Klawonn et al. 2015; Chang et al. 2019), the $^{15}\text{N}_2$ tracer was added by bubble injection and subsequent release. First, 4 mL of $^{15}\text{N}_2$ gas (99 atom %, Cambridge Scientific, LOT # I-19197/AR0586172) was injected into each 4.4 L incubation bottle using a gas-tight syringe inserted through a silicone septum on the bottle cap. Incubation bottles were then rotated on a customized plankton wheel for 15 min at 17 rpm to facilitate $^{15}\text{N}_2$ gas equilibration. Next, the cap was opened to release the residual $^{15}\text{N}_2$ bubble, and a 1 mL of sample was removed and

transferred to a pre-evacuated Exetainer® pre-loaded with 85% phosphoric acid for later analysis of the isotopic composition of dissolved inorganic C. A second subsample was transferred to a 20 mL serum vial using a peristaltic pump and a tube extending to the bottom of incubation bottles. This sample was collected for later measurement of the initial atom % of N_2 via MIMS as per Ferrón et al. (2016), which averaged $2.66 \pm 0.47\%$ among all incubation bottles. The incubation bottle was then filled to capacity with seawater from the sampling site, capped, and incubated as described above.

$^{15}\text{N}_2$ fixation rates were calculated as described by Montoya et al. (1996). Limits of detection (LOD) and minimum quantifiable rates (MQRs) for N_2 fixation measurements were calculated for each water mass, as described by Gradoville et al. (2017) (Table S1).

UCYN-A cell-specific NFRs

During the 2017 cruise, subsamples from community NFR incubation bottles were preserved in order to measure single-cell NFRs by the cyanobacterium UCYN-A. Immediately prior to filtration, 95 mL from both the $^{15}\text{N}_2$ incubation bottles and the time zero $\delta^{15}\text{N}$ natural abundance bottles were subsampled into amber bottles and fixed with 5 mL of 37% filtered formaldehyde. Fixed samples were stored at 4°C for up to 48 h, then gently vacuum-filtered onto a 25 mm, $0.6\ \mu\text{m}$ pore size Isopore polycarbonate filter (EMD Millipore, Hayward) with a 25 mm, $0.8\ \mu\text{m}$ pore cellulose acetate backing filter (Sterlitech, Kent). Filters were rinsed, dried, and stored at -80°C .

UCYN-A associations were visualized using a double-catalyzed reporter deposition fluorescence in situ hybridization (CARD-FISH) assay. This assay involved two separate hybridizations, one to label UCYN-A, using the oligonucleotide probe UCYN-A 732 and helper oligonucleotides Helper A-732 and Helper B-732 (Krupke et al. 2013), and one to label the haptophyte host, using the probe UPRYM69 and helper oligonucleotides Helper A-PRYM and Helper B-PRYM (Cornejo-Castillo et al. 2016). The CARD-FISH assay was performed as described by Cabello et al. (2016), but without the use of competitor oligonucleotides. After the hybridizations, filter pieces were washed in MilliQ to remove mounting media, and cells were transferred to conductive, gridded silicon wafers (Pelcotec SFG12 Finder Grid Substrate, Ted Pella, Redding) by wetting filter pieces with 10 μL of MilliQ, placing the filter pieces face down on the silicon wafers, freezing at -80°C , and quickly removing the filter pieces while the sample was still frozen. UCYN-A1 associations were identified, imaged, and mapped (see Dekas and Orphan 2011) using a Zeiss Axioplan epifluorescence microscope (Santa Cruz, CA). Only intact associations containing fluorescent label for both the host and symbiont were used for analyses. Additionally, only those symbioses with diameters $<4\ \mu\text{m}$ were analyzed in order to target UCYN-A1 associations and not the larger UCYN-A3 associations (which were rare in our samples).

The C and N isotopic compositions of UCYN-A associations were measured using nanoscale secondary ion mass

Table 1. Ranges of physical, chemical, and biological conditions of seawater sampled from stations in the NPSG and the NPTZ during the 2016 and 2017 cruises.

Cruise	Region	Number of stations	Latitude (°N)	SST* (°C)	SSS [†]	N + N (μmol L ⁻¹)	PO ₄ (μmol L ⁻¹)	Chl [‡] (mg m ⁻³)	Fe (nmol kg ⁻¹)
April–May 2016	NPSG	6	23.5–29.7	19.8–24.0	35.1–35.3	Bd [§] -0.002	0.02–0.05	0.10–0.11	0.26–0.51
	NPTZ	8	32.6–37.3	11.4–17.1	34.1–34.7	0.06–5.87	0.07–0.51	0.16–0.37	0.06–0.18
May–June 2017	NPSG	11	25.8–32.3	19.8–24.2	34.8–35.3	0.001–0.01	0.03–0.05	0.04–0.08	0.11–0.31
	NPTZ	18	32.9–41.4	11.0–18.0	33.0–34.4	0.002–1.99	0.07–0.51	0.05–3.33	0.11–0.51

*SST indicates sea surface temperature.

[†]SSS indicates sea surface salinity.

[‡]Calibrated concentrations of chlorophyll *a* (2016) and chlorophyll *a* (2017) from CTD fluorometer.

[§]Bd indicates below detection limits.

spectrometry (nanoSIMS). A total of 79 UCYN-A associations were analyzed (10–12 cells per sample). All measurements were performed using a Cameca NanoSIMS 50L at the Stanford Nano Shared Facilities laboratory (<http://snsf.stanford.edu>) at Stanford University. Cells were located and presputtered with a large diameter beam of cesium ions (Cs⁺) for 2 min to remove impurities and implant Cs⁺ on the cell surface, and the Cs⁺ was focused to a <100-nm spot diameter. For the analysis, cells were rastered (16 keV with a current between 2 and 4 pA) over a 25 × 25 μm area with a dwelling time of ~1 ms per pixel, producing a 256 × 256 pixel image. Secondary anions of ¹²C¹⁴N⁻, ¹²C¹⁵N⁻, ¹²C⁻, ¹³C⁻, ¹⁶O⁻, ²⁸Si⁻, and ³¹P⁻ were collected simultaneously, along with a secondary electron image (1 AU). Thirty frames were imaged for each individual cell. The look@nanoSIMS software (Polerecky et al. 2012) was used to accumulate the plane images and draw regions of interest (ROIs) around UCYN-A associations using the look@nanoSIMS automatic thresholding feature (both host and symbiont were analyzed together as a single association). The ¹⁵N/¹⁴N ratio was calculated for each ROI (as ¹²C¹⁵N/¹²C¹⁴N), and cell diameters were estimated from the perimeter of each ROI, assuming a spherical shape.

NFRs by UCYN-A associations (both host and symbiont together) were calculated according to Montoya et al. (1996), with the modification that the particulate N concentration ([PN]) term was replaced with the N content per UCYN-A association. This term was estimated by calculating the cell volume (assuming a spherical shape), estimating cellular C content using a previously derived equation relating cellular C content to biovolume in haptophytes (Strathmann 1967; Krupke et al. 2015), and converting cellular C content to cellular N content assuming a molar C:N ratio of 6.3 for UCYN-A associations (Martinez-Perez et al. 2016). For the initial atom% PN term (T_{initial}), we used the mean value of 32 analyzed unenriched symbioses (0.38 ± 0.0066 atom% ¹⁵N). Detection limits for cell-specific rates were determined by setting a minimum change in atom% ¹⁵N through the incubation ($T_{\text{final}} - T_{\text{initial}}$), which was calculated as 3 times the standard deviation of the atom% ¹⁵N of unenriched T_{initial} cells (0.0199 atom%, $n = 32$ cells).

Statistical analyses

Model II linear regressions (ordinary least squares method) were used to test the relationships between the abundances of diazotrophic taxa and community NFRs, and between UCYN-A1 abundances and environmental variables. Regressions were performed using the lmodel2 package version 1.7.3 (Legendre 1998) in the program R (version 3.4.1; <http://www.r-project.org/>).

Results

Oceanographic conditions

We collected samples from two springtime meridional surveys through the NPSG and the NPTZ. Both cruises sampled strong gradients in physical, chemical, and biological features (Table 1). Sea surface temperature decreased gradually with increasing latitude, ranging from 11.4 to 24.0°C in 2016 and from 11.0 to 26.2°C in 2017. Sea surface salinity ranged from ~34.8 to 35.3 in the NPSG, then abruptly decreased at ~30.5°N to reach ~34.3 at ~33°N (Fig. 2). This surface salinity gradient

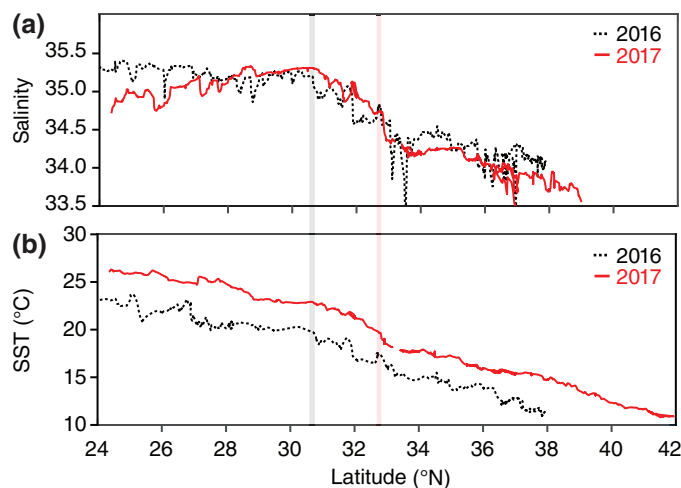


Fig. 2. Sea surface salinity (a) and temperature (SST, b) on the 2016 and 2017 transects. Vertical lines delineate the boundary between the NPSG and the NPTZ during the 2016 (gray) and 2017 (red) cruises.

is indicative of the southern boundary of the subtropical frontal zone (Roden 1991) and encompassed the 18°C isotherm during both cruises. Here, we have used the second derivative of surface salinity as a delineation between the NPSG and NPTZ, corresponding to 30.7°N in 2016 and 32.8°N in 2017 (Fig. 2). Sea surface salinity decreased below 33.8 north of 38°N during the 2017 cruise, indicative of the subpolar frontal zone (Fig. 2, Roden 1991). The vertical structure of salinity supports our regional delineations: stations south of ~32°N had a saline

surface layer, indicating the subtropical domain, stations north of ~38°N had a low-salinity surface layer, reflecting the influence of the subarctic domain, and stations between ~32°N and 38°N show a mixture of these two water types, indicating the transition zone (Supporting Information Fig. S1, Roden 1991). Temperature/salinity curves from NPSG stations reflect typical curves from the subtropical gyre, while stations in the NPTZ progressively show characteristics more similar to the subarctic gyre (Supporting Information Fig. S2).

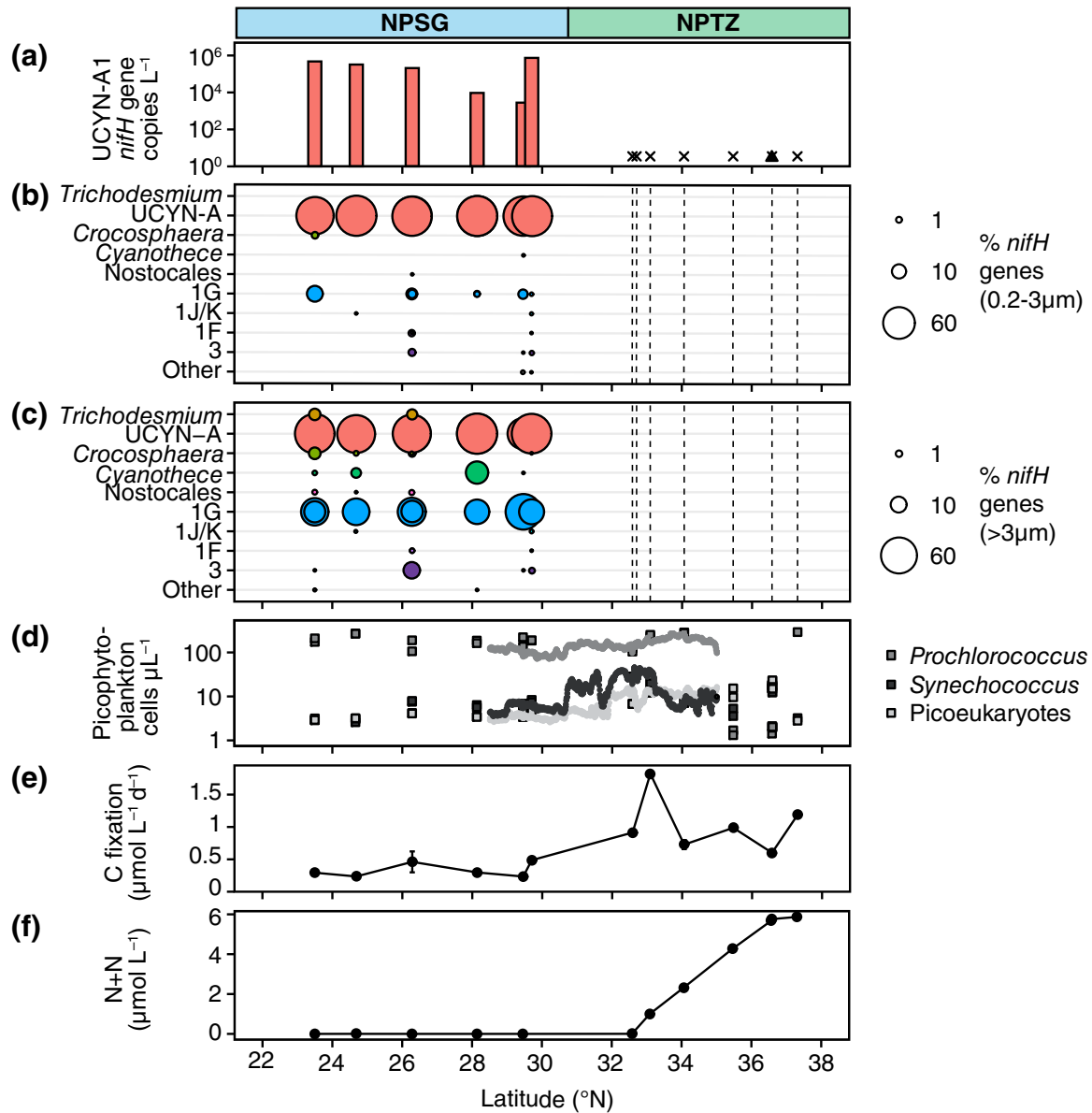


Fig. 3. Abundances of *nifH* genes and biogeochemical conditions during the 2016 transect (~158°W). UCYN-A1 *nifH* gene abundances (via qPCR) are presented in (a), with 'x's and triangles representing samples below the limit of detection or quantification, respectively. The relative abundances of diazotrophic taxa (via *nifH* gene sequencing) from two size fractions are shown in (b) and (c), with vertical dashed lines indicating samples for which no *nifH* genes were recovered. Concentrations of picophytoplankton (via discrete flow cytometry samples [squares] and continuous SeaFlow measurements, (d), ¹³C primary production rates (e), and nitrate+nitrite concentrations (f) are shown for biogeochemical context. The division between the NPSG and NPTZ is presented in the upper panel.

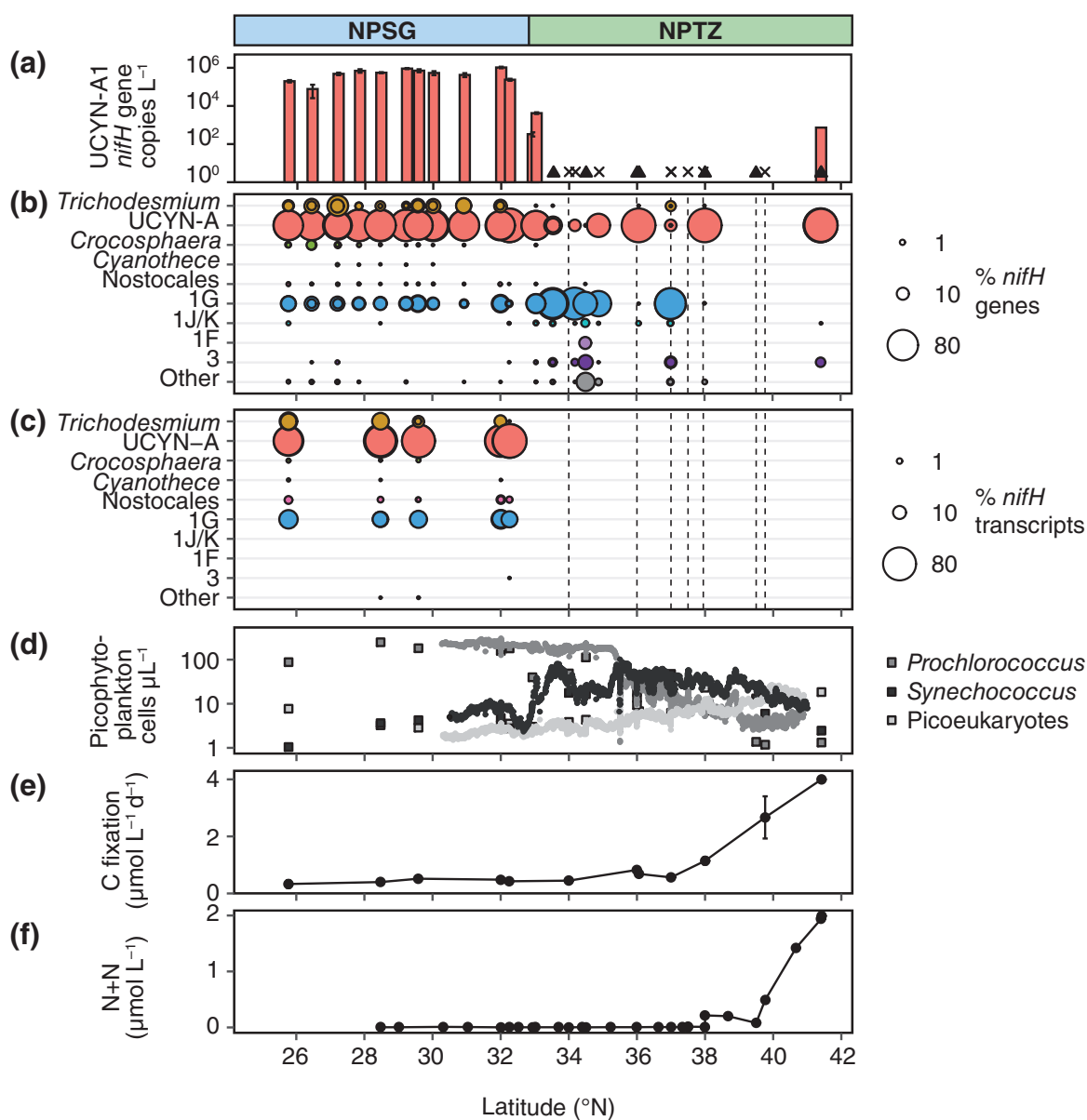


Fig. 4. Abundances of *nifH* genes and biogeochemical conditions during the 2017 transect (~158°W). UCYN-A1 *nifH* gene abundances (via qPCR) are presented in (a), with x's and triangles representing samples below the limit of detection or quantification, respectively. The relative abundances of diazotrophic taxa from sequencing *nifH* genes and transcripts are shown in (b) and (c), with vertical dashed lines indicating samples for which no *nifH* genes were recovered. Concentrations of picophytoplankton (via discrete flow cytometry samples [squares] and continuous SeaFlow measurements), (d), ^{13}C primary production rates (e) and nitrate+nitrite concentrations (f) are shown for biogeochemical context. The division between the NPSG and NPTZ is presented in the upper panel.

Inorganic nutrient and dissolved iron concentrations varied with latitude. Concentrations of N + N and SRP were low in the NPSG (≤ 10 and ≤ 55 $nmol L^{-1}$, respectively), and increased sharply in the NPTZ during both cruises (Table 1, Figs. 3, 4). The latitudinal trend for dissolved iron concentrations differed between the two surveys (Table 1). In the 2016 cruise, dissolved iron concentrations were highest in the NPSG (0.26 – 0.51 $nmol kg^{-1}$) and decreased steadily with latitude to a minimum of ~ 0.06 $nmol kg^{-1}$. In contrast, during the 2017 cruise, the highest dissolved iron

concentrations were observed in NPTZ stations south of the subpolar frontal zone (0.20 – 0.51 $nmol kg^{-1}$), while concentrations were lower in the NPSG (0.11 – 0.31 $nmol kg^{-1}$) and in the subpolar frontal zone (0.11 – 0.41 $nmol kg^{-1}$) (P. Pinedo, unpublished data).

The community structure of picophytoplankton had strong latitudinal patterns. Concentrations of picophytoplankton were relatively stable among NPSG stations, with high concentrations of *Prochlorococcus* (114.3 ± 9.3 and 137.9 ± 18.9 $cells \mu L^{-1}$ in 2016 and 2017, respectively) and lower concentrations of

Synechococcus (8.9 ± 2.3 and 3.2 ± 1.2 cells μL^{-1} in 2016 and 2017, respectively) and picoeukaryotes (5.5 ± 2.6 and 2.5 ± 1.8 cells μL^{-1} in 2016 and 2017, respectively) (Figs. 3, 4). The concentrations of *Synechococcus* and picoeukaryotes increased 5–10-fold at the southern edge of the NPTZ (30.5°N in 2016 and 32.8°N in 2017), reaching >35 cells μL^{-1} for *Synechococcus* and >27 cells μL^{-1} for picoeukaryotes in both years (Figs. 3, 4). In the northern portion of the NPTZ, *Prochlorococcus* dropped by two orders of magnitude at around $\sim 35^\circ\text{N}$ in both years and concentrations of *Synechococcus* decreased \sim two-fold north of $\sim 33.5^\circ\text{N}$ in 2016 (18.4 ± 11.3 cells μL^{-1}) and $\sim 39.5^\circ\text{N}$ in 2017 (9.6 ± 6.8 cells μL^{-1}), while concentrations of picoeukaryotes remained relatively high (22.8 ± 6.0 and 10.8 ± 4.4 cells μL^{-1} in 2016 and 2017, respectively).

Chloropigment fluorescence and ^{13}C primary production varied strongly with latitude. Chloropigment concentrations were low (<0.1 mg m^{-3}) in the subtropical gyre and increased with latitude across the NPTZ; the transition zone chlorophyll front (0.2 mg m^{-3}) was observed at $\sim 32^\circ\text{N}$ in 2016 and at $\sim 36^\circ\text{N}$ in 2017 (Table 1). ^{13}C fixation rates ranged from 0.2 to 1.8 $\mu\text{mol C L}^{-1} \text{ d}^{-1}$ during the 2016 cruise and from 0.3 to 4.0 $\mu\text{mol C L}^{-1} \text{ d}^{-1}$ during the 2017 cruise; rates increased with latitude across the NPTZ during both cruises (Figs. 3, 4). The highest ^{13}C fixation rates were observed in the subpolar frontal zone during 2017 (the northernmost stations sampled in this study). Because ^{13}C samples were not fumed to remove inorganic carbon, we have compared our ^{13}C fixation rates to ^{14}C measurements conducted on the same cruise (A. White, unpublished data). The two sets of measurements correlate well ($R^2 = 0.96$ and 0.93 for 2016 and 2017 cruises, respectively) and show similar latitudinal patterns in the magnitude of production estimates (data not shown).

Diazotrophic diversity, abundance, and distribution

Diversity of *nifH* genes and transcripts

The diversity of marine diazotrophs was assessed via high-throughput sequencing of partial *nifH* genes and transcripts. Four different types of samples were sequenced: small size-fraction (0.2 – 3 μm) 2016 DNA samples, large size fraction (>3 μm) 2016 DNA samples, nonfractionated (>0.2 μm) 2017 DNA samples, and nonfractionated 2017 cDNA samples. A total of 140 samples containing 227 OTUs remained after quality control procedures and rarefaction. These OTUs clustered with all four *nifH* gene clades (Zehr et al. 2003), with the majority (94%) of sequences assigned to groups 1B (cyanobacteria) or 1G (mostly gamma-proteobacteria) (Figs. 2, 3). The diazotrophic group with the highest relative abundance in all sample types was the symbiotic cyanobacterium UCYN-A.

In the 2016 cruise, *nifH* genes were successfully amplified from 26/32 small size fraction NPSG samples and from 28/32 large size fraction NPSG samples but were not amplified from NPTZ samples of either size fraction (absence of visual band after gel electrophoresis). Within the NPSG, *nifH* gene sequences from surface waters were numerically dominated by UCYN-A in

both the small and large size fractions (Fig. 3). Other cyanobacterial groups included *Trichodesmium*, *Crocospaera*, *Cyanothece* and members of the order Nostocales. Of non-cyanobacterial *nifH* sequences, the most frequently detected group in surface samples was the gamma-proteobacterial group 1G. This group includes OTUs that match qPCR primer/probe sets designed to target several uncultivated diazotrophic phylotypes, including the globally distributed group “Gamma-A” (Church et al. 2005a; Langlois et al. 2008; Langlois et al. 2015), as well as phylotypes previously observed in the South Pacific (ETSP-2 and Gamma-3, Halm et al. 2011; Turk-Kubo et al. 2014). The community composition of diazotrophs shifted with depth; for example, the noncyanobacterial *nifH* group 3 (putative anaerobes) and the cyanobacterium *Cyanothece* displayed the highest relative abundances near the base of the euphotic zone (Supporting Information Fig. S3). There were higher relative abundances of genes from large cyanobacteria (*Trichodesmium* and members of the order Nostocales), *Cyanothece*, *Crocospaera*, and noncyanobacterial groups in the large size fraction (Fig. 3, Supporting Information Fig. S3).

During the 2017 cruise, *nifH* genes were successfully amplified from 52/54 NPSG samples and from 22/110 NPTZ samples. Within the gyre, *nifH* gene sequences from surface seawater were dominated by UCYN-A, followed by group 1G and *Trichodesmium* (Fig. 3). In the NPTZ samples for which the *nifH* gene was amplified, UCYN-A and group 1G again had the highest relative abundances. However, there were higher relative abundances of group 1G and other noncyanobacterial groups in the NPTZ than in the NPSG. Furthermore, while cyanobacteria other than UCYN-A (*Trichodesmium*, *Crocospaera*, *Cyanothece*, and the members of Nostocales) were detected in most surface NPSG samples, these groups were rarely or never detected in NPTZ samples. Likewise, overall diazotrophic species richness was lower in the NPTZ than in the NPSG (Supporting Information Fig. S4).

The community structure of active diazotrophs was assessed in 2017 using RNA samples collected from surface seawater. *nifH* transcripts were amplified from all NPSG samples but were not amplified from any NPTZ samples. Within the NPSG, the diazotrophic community composition of *nifH* transcripts was similar to that of surface *nifH* genes, with the majority of transcripts belonging to UCYN-A. Transcripts belonging to other cyanobacterial groups (*Crocospaera*, *Cyanothece*, and the members of Nostocales) and to group 1G were also present in NPSG samples (Fig. 4).

Abundances of marine diazotrophs

Quantitative PCR was used to enumerate the *nifH* genes of nine diazotrophic groups from surface seawater samples in order to assess the quantitative significance of dominant diazotrophic taxa. In the 2016 cruise, *nifH* genes were detected in the six NPSG stations but were below the limit of detection or quantification in all samples from the NPTZ. Within the NPSG, the most abundant group was UCYN-A1, whose

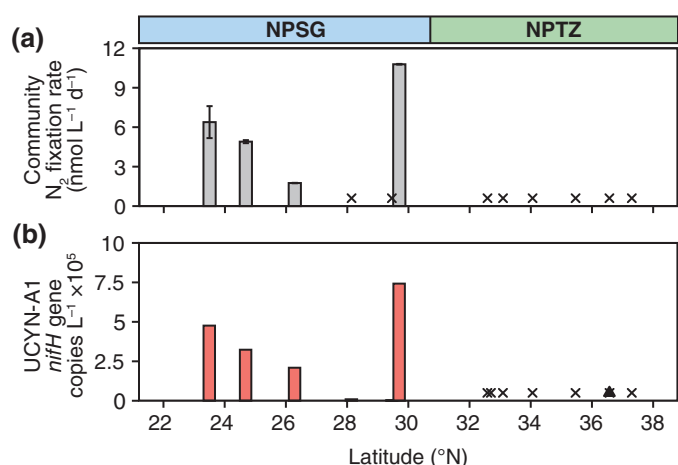


Fig. 5. Community N_2 fixation rates (a) and UCYN-A1 *nifH* gene abundances (b) during the 2016 cruise. X's denote below limit of detection; triangles denote below limit of quantification. The division between the NPSG and NPTZ is presented in the upper panel.

abundances ranged from 2.8×10^3 to 7.3×10^5 *nifH* gene copies L^{-1} and from below quantification limits to 9.7×10^3 *nifH* gene copies L^{-1} in the small and large size fractions, respectively (Figs. 3, 5). The groups UCYN-B, UCYN-A2/A3, UCYN-C, het-1, het-2, and Gamma-A were also detected at low

abundances (all $<4.0 \times 10^3$ *nifH* gene copies L^{-1}) in some NPSG samples (Supporting Information Table S2).

In the 2017 cruise, only UCYN-A1 and *Trichodesmium nifH* gene abundances were quantified. UCYN-A1 *nifH* genes were detected in surface samples from all NPSG stations, with abundances ranging from 7.8×10^4 to 1.0×10^6 *nifH* gene copies L^{-1} (Figs. 3, 6). UCYN-A1 abundances were below either the limit of detection or the limit of quantification for most surface NPTZ stations, with the exception of two stations at the southern edge of the NPTZ and the northernmost station, which all had low UCYN-A1 abundances ($<5 \times 10^3$ *nifH* gene copies L^{-1}). *Trichodesmium nifH* genes were detected in surface waters from 11/12 NPSG stations (2.8×10^3 – 2.8×10^5 *nifH* copies L^{-1}) but were below limits of detection or quantification at all NPTZ stations (Supporting Information Table S2). Since diazotrophs other than UCYN-A1 were detected sporadically and at low abundances during both cruises, this manuscript primarily focuses on the patterns observed for UCYN-A1.

Community NFRs

Community $^{15}\text{N}_2$ fixation rates varied with latitude during both cruises. Different methods were used to introduce the $^{15}\text{N}_2$ tracer on the two cruises (see *Methods*); LOD ranged from 0.27 to 0.90 $\text{nmol N L}^{-1} \text{d}^{-1}$ in 2016 and from 0.33 to 0.59 during 2017 (Supporting Information Table S1). During the 2016 cruise, surface NFRs were detected in 4/6 NPSG stations and ranged from 1.75 to 10.8 $\text{nmol N L}^{-1} \text{d}^{-1}$ (Fig. 5). Rates were below LOD in two northern NPSG stations as well as in all stations within the NPTZ. The NFR at one NPSG station during the 2016 cruise was above LOD but below MQR; this rate was retained for analyses (Stn. 14, Supporting Information Table S1). During the 2017 cruise, surface NFRs were detected at all stations within the NPSG. Rates in this region ranged from 10.2 to 20.8 $\text{nmol N L}^{-1} \text{d}^{-1}$, approaching the upper bound of the range of ~ 0 – 20 $\text{nmol N L}^{-1} \text{d}^{-1}$ reported at

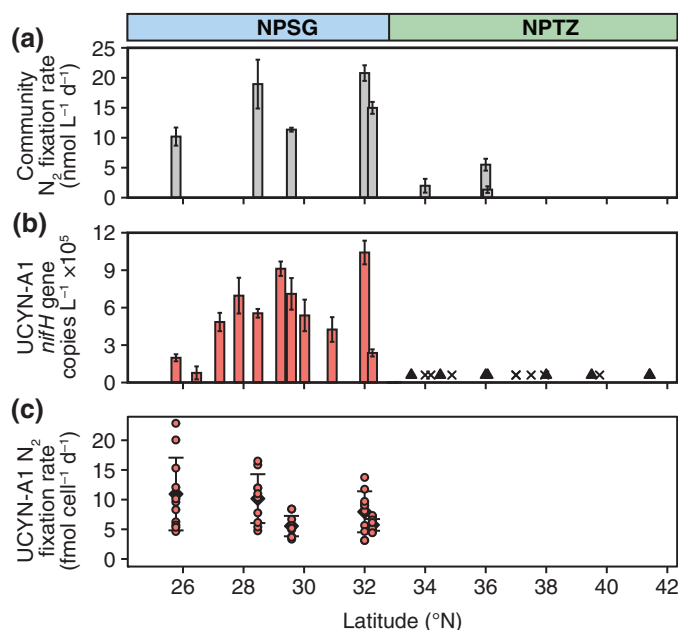


Fig. 6. Community N_2 fixation rates (NFRs) (a), UCYN-A1 *nifH* gene abundances (b), and UCYN-A1 cell-specific NFRs (c) during the 2017 cruise. X's denote below limit of detection; triangles denote below limit of quantification. Note that community NFR assays were not performed at stations north of 36°N during 2017. Each circle in (c) represents the rate measured from an individual UCYN-A association, while the diamonds and error bars represent the mean and standard deviation, respectively ($n = 10$ – 12 symbioses analyzed per sample).

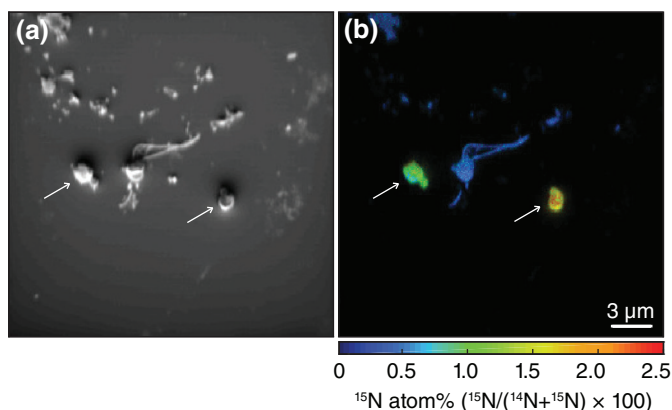


Fig. 7. Secondary electron image (a) and ^{15}N enrichment (b) of two UCYN-A associations (indicated with white arrows) from the NPSG during the 2017 cruise. Images were produced from nanoSIMS measurements of UCYN-A symbioses after natural communities had been incubated with $^{15}\text{N}_2$ gas.

Station ALOHA (Fig. 6, Böttjer et al. 2017). In the NPTZ, NFRs were lower (1.35–5.52 nmol N L⁻¹ d⁻¹) but above LOD at all stations in which the assays were performed. The ratio of N₂ fixation to C fixation ranged from 3.1 to 4.8% in the NPSG and from 0.20 to 0.67% in the NPTZ (Supporting Information - Table S3). No N₂ fixation assays were performed at stations north of 36°N during 2017.

UCYN-A cell-specific NFRs

UCYN-A cell-specific NFRs were measured during the 2017 cruise using CARD-FISH and nanoSIMS (Fig. 7). CARD-FISH assays were performed using samples from all eight stations in which ¹⁵N₂ incubations were conducted. UCYN-A associations were only located on those filters from the five NPSG stations, presumably due to low cell abundances in the three NPTZ stations where UCYN-A1 *nifH* genes were below the limit of quantification. Therefore, UCYN-A cell-specific NFRs in the NPTZ could not be assessed. Within the NPSG, NFRs of individual UCYN-A associations ranged from 3.09 to 22.8 fmol N cell⁻¹ d⁻¹; average cell-specific rates from each station ranged from 5.7 to 10.9 fmol N cell⁻¹ d⁻¹ (Fig. 6). These rates are within the ranges of cell-specific rates by UCYN-A associations of this ecotype (UCYN-A1) previously reported in the North Atlantic Ocean and the Arctic Ocean (Martinez-Perez et al. 2016; Harding et al. 2018). All measured cell-specific NFRs exceeded detection limits, which ranged from 0.07 to 0.13 fmol N cell⁻¹ d⁻¹.

Table 2. *R*² values from simple linear regressions of community NFR vs. *nifH* gene abundances of diazotrophic groups in surface seawater. Regressions were run using the full data set and also separately for NPSG stations only. During 2016 nine diazotrophic *nifH* phylotypes were quantified, while in 2017 only the two diazotrophic groups with the highest relative abundances (via *nifH* gene sequencing) were targeted. Significant correlations (*p* < 0.05) are highlighted in bold text. The groups *Trichodesmium* and het-3 were below the LOD or LOQ in all samples.

Cruise	Target organism	<i>R</i> ² value (all stations)	<i>R</i> ² value (NPSG only)
2017	UCYN-A1	0.693	0.380
	<i>Trichodesmium</i>	0.428	0.212
2016	UCYN-A1	0.988	0.984
	UCYN-B	0.173	0.08
	UCYN-A2/A3	0.239	0.07
	UCYN-C	0.152	0.04
	<i>Trichodesmium</i>	(Below LOD or LOQ)	(Below LOD or LOQ)
	het-1	0.100	0.00
	het-2	0.250	0.09
	het-3	(Below LOD or LOQ)	(Below LOD or LOQ)
	Gamma-A	0.164	0.08

Correlations among UCYN-A abundances, NFRs, and ocean biogeochemistry

Community NFRs correlated strongly with surface UCYN-A1 *nifH* gene abundances on both cruises (*R*² = 0.99, *p* < 0.001 and *R*² = 0.69, *p* = 0.01 on the 2016 and 2017 cruises, respectively) and did not correlate significantly with the *nifH* gene abundances of any other quantified diazotrophic group (Table 2). The UCYN-A cell-specific NFRs (measured in 2017 only) did not correlate with UCYN-A1 *nifH* gene abundances (*R*² = 0.05, *p* = 0.73) or with community NFRs (*R*² = 0.005, *p* = 0.92).

There were significant correlations between UCYN-A1 *nifH* gene abundances and environmental parameters (Supporting Information Table S4). Using data from both cruises, UCYN-A1 *nifH* gene abundances correlated with sea surface temperature (*R*² = 0.72, *p* < 0.001) and inversely correlated with latitude (*R*² = 0.59, *p* < 0.001). No significant correlations were found with UCYN-A1 *nifH* gene abundances and other measured abiotic environmental parameters. When restricting regression analyses to each year separately, UCYN-A1 *nifH* gene abundances correlated with dissolved iron concentration in 2016 (*R*² = 0.73, *p* = 0.002) but inversely correlated with dissolved iron concentration in 2017 (*R*² = 0.72, *p* < 0.001). When restricting regression analyses to NPSG stations only, there were no significant correlations between UCYN-A1 *nifH* gene abundances and any measured environmental parameter (Supporting Information Table S4).

Discussion

Boundaries for diazotrophy within the North Pacific transition zone

In the NPTZ, the southward Ekman transport of cold, nitrate-rich subarctic surface waters is generally assumed to favor the growth of large cell size, fast-growing phytoplankton over diazotrophs (e.g., Dutkiewicz et al. 2012). However, increasing reports of active marine diazotrophs in unexpected environments, including cold and high-nitrate waters (Shiozaki et al. 2017), show that the biogeography and environmental controls of marine N₂ fixation need to be re-evaluated. Here, we present two springtime meridional surveys of diazotrophic abundance, diversity, and activity through the environmental gradients of the NPTZ. We found a clear boundary for diazotrophs near the subtropical frontal zone that defines the southern-most edge of the NPTZ. South of the front, *nifH* genes, transcripts, and NFRs were consistently detected, and north of the front, *nifH* genes were rare or absent and NFRs were low or undetected. Our study expands on previous observations of low diazotrophic abundances in the NPTZ (Church et al. 2008; Shiozaki et al. 2017) and raises questions about the environmental factors that restrict the abundance and activity of diazotrophs in the NPTZ yet retain diazotrophs as members of the rare biosphere.

The high sampling resolution during the 2017 cruise revealed a sharp diazotrophic boundary at ~33.5°N, north of

which abundances of UCYN-A decreased by orders of magnitude (Fig. 4). This coincided with a sharp increase in *Synechococcus* abundance. Temperature/salinity curves indicate the transition to a new water mass near this station (Supporting Information Fig. S2); thus, the abrupt shift in abundances of UCYN-A and *Synechococcus* likely reflects low mixing rates at the physical front between water masses. While our sampling resolution was coarser during the 2016 cruise, the northern boundary for UCYN-A was likewise near the subtropical frontal zone at the southern edge of the NPTZ.

The underlying drivers of the lower diazotroph abundances and NFRs north of this front are unclear. Much of this uncertainty stems from the fact that the dominant diazotroph in our samples was UCYN-A, an uncultivated cyanobacterium that lives in an unusual, poorly understood symbiosis with a prymnesiophyte alga (Zehr et al. 2016). While most aspects of UCYN-A ecology are unresolved, there is evidence that the ecological controls of this organism may diverge from those of other cyanobacterial diazotrophs. For instance, temperature is a known control of marine N_2 fixation (Luo et al. 2014), and the temperature at 33.5°N during the 2017 cruise (~18°C) was near the lower thermal limit for *Trichodesmium* growth (e.g., Breitbarth et al. 2007). Temperature has been predicted to restrict N_2 fixation in the NPTZ (Wang et al. 2019), and may help explain the absence of certain cyanobacterial diazotrophs from the region. However, members of the same UCYN-A lineage dominant in our study (UCYN-A1) were recently shown to actively fix N_2 in the Arctic Ocean at temperatures as low as 4.1°C (Harding et al. 2018). In our study, UCYN-A abundance correlated strongly with sea surface temperature across the full transect, but within the NPTZ, the highest UCYN-A *nifH* gene abundances were detected at the northernmost station, where temperatures were coldest. Thus, the reduced temperatures in the NPTZ relative to the NPSG do not explain the abrupt shift in UCYN-A between these two ecosystems; instead, the broad temperature tolerance of UCYN-A may enable this organism to remain rare but active in NPTZ waters.

The availability of fixed N is another environmental control for which the response of UCYN-A may diverge from responses of other cyanobacterial diazotrophs. Nitrate availability has been suggested to suppress diazotrophy due to the higher energetic cost of N_2 fixation relative to nitrate uptake, direct inhibition, or elevated N : P ratios (Falkowski 1983; Ohki et al. 1991; Knapp 2012). However, short-term deck-board incubation experiments have shown that UCYN-A growth rates may increase following nitrate additions (Turk-Kubo et al. 2018). The effects of macronutrients on the UCYN-A symbiosis are not fully understood, especially in the context of long-term nutrient delivery experienced in situ. In our study, the northern boundary for UCYN-A was not coincident with measurable changes in macronutrient concentrations (Figs. 3, 4) or in N : P ratios (data not shown), and UCYN-A abundances did not correlate with N + N or N : P (Table S4). It is possible that potentially higher nitrate supply rates in the NPTZ may have

supported the growth of nondiazotrophic phytoplankton over diazotrophic taxa including UCYN-A (e.g., high N : Fe or N : P supply ratio, Dutkiewicz et al. 2012; Ward et al. 2013). Top-down processes and/or physiological constraints on the prymnesiophyte host may also play an important role in limiting the abundances of UCYN-A in the NPTZ.

Although community NFRs in the NPTZ were lower than those we measured in the NPSG, NFRs were consistently detected across the NPTZ in the 2017 cruise (Fig. 6). This result agrees with the low NFRs predicted in the NPTZ by two separate models in a recent study by Wang et al. (2019) but contrasts with outputs of several global N_2 fixation models that predict an absence of diazotrophy in the region (Deutsch et al. 2007; Ward et al. 2013). The low N_2 : C fixation ratios in the NPTZ observed here (Supporting Information Table S3) and previously (Shiozaki et al. 2017) imply that N_2 fixation contributes a small fraction of new N to the euphotic zone and is likely of low biogeochemical significance to the region. Nevertheless, our results add to a growing literature documenting marine N_2 fixation in temperate and high-latitude environments (e.g., Rees et al. 2009; Blais et al. 2012; Mulholland et al. 2012; Shiozaki et al. 2017, 2017; Harding et al. 2018).

There are several possible explanations for why diazotrophic genes and low NFRs were detected in the NPTZ in 2017 but not in 2016. First, the 2017 cruise was ~1.5 months later in year. The NPTZ exhibits extreme seasonality, so this moderate difference in the timing of the 2017 expedition corresponded to large shifts in macronutrient concentrations, pico-phytoplankton community composition, and ^{13}C primary productivity (Figs. 3, 4). There were also differences in distributions of dissolved iron: during 2016, iron concentrations increased from north to south, but in 2017, the highest iron concentrations were observed in the NPTZ, likely driven by abnormally high inputs of aeolian dust (P. Pinedo, unpublished data). Since the availability of iron is a major constraint of marine N_2 fixation, especially in the Pacific Ocean (Weber and Deutsch 2014), the higher iron concentrations in 2017 may have facilitated increased rates of diazotrophic growth and N_2 fixation. Finally, differences in methodologies used on the two cruises could also contribute to the observed differences in the NPTZ. During 2016, DNA samples were size-fractionated and smaller filtration volumes were used, which likely decreased the likelihood of detecting rare *nifH* genes. Additionally, different methods were used to introduce the $^{15}N_2$ tracer on the two cruises (see Methods), which could have contributed to observed differences in community NFRs. Still, despite the difference in the magnitude of rates and gene abundances, both surveys showed the same overall feature of low or undetectable *nifH* gene abundances and NFRs in the NPTZ.

It is not clear which diazotrophic taxa drove the observed NFRs in the NPTZ during the 2017 cruise. Diazotrophic species richness was low in the NPTZ (Supporting Information Fig. S4). UCYN-A *nifH* genes were recovered from stations farther north than those of other cyanobacterial diazotrophs (up to 41.5°N),

consistent with recent findings indicating that UCYN-A broadens the geographic range of diazotrophic cyanobacteria (Moisander et al. 2010; Harding et al. 2018). However, abundances of UCYN-A were below the limit of quantification in most NPTZ samples (<500 *nifH* copies L^{-1}). Assuming the highest UCYN-A cell-specific NFR measured in the NPSG (10.9 $fmol\ N\ cell^{-1}\ d^{-1}$), it would require 1.4×10^5 UCYN-A cells to account for the lowest community NFR measured in the NPTZ (1.35 $nmol\ N\ L^{-1}\ d^{-1}$, Fig. 6). Thus, it is unlikely that this UCYN-A sublineage (UCYN-A1) was responsible for all, or even most, of community N_2 fixation in this region. Stations from the NPTZ also contained higher relative abundances of *nifH* genes from noncyanobacterial diazotrophs, but few of these organisms exist in culture and their biogeochemical significance is not well understood (Moisander et al. 2017). Surprisingly, *nifH* transcripts were not recovered from any NPTZ stations, and *nifH* genes were not recovered from the NPTZ station with the highest NFR (Figs. 4, 6). Shiozaki et al. (2017) likewise reported the detection of N_2 fixation but not *nifH* genes (via qPCR) in the NPTZ. Similar enigmatic N_2 fixation has been observed in the South Pacific (Turk-Kubo et al. 2014; Gradoville et al. 2017) and suggests that ecologically important groups of diazotrophs are not targeted using the current *nifH* PCR primers (Cornejo-Castillo 2017; Delmont et al. 2018).

Finally, it could be hypothesized that some diazotrophs detected in the NPTZ were advected horizontally from their habitat and may not be active in the NPTZ. A recent study by Cheung et al. (2019) found that diazotrophs are advected through the Kuroshio current, and that in particular, the UCYN-A1 lineage and noncyanobacterial diazotrophs can be advected large distances. While the NPTZ stations sampled in our study do not show temperature/salinity attributes that implicate Kuroshio extension source waters (Supporting Information Fig. S2), the Kuroshio Extension is the origin of the North Pacific Current that flows east through the NPTZ (Yasuda 2003; Hu et al. 2015) and we cannot rule out the possibility that UCYN-A or other diazotrophs were delivered by horizontal advection. Physical transport may likewise explain previous observations of cyanobacterial diazotrophs at high latitudes in the North Atlantic (e.g., Lipschultz and Owens 1996; Díez et al. 2012; Rivero-Calle et al. 2016).

UCYN-A dynamics within the North Pacific subtropical gyre

The NPSG is one of the best-studied habitats for marine diazotrophs. While early work in the NPSG focused on *Trichodesmium* and heterocystous cyanobacterial symbionts of diatoms (Mague et al. 1974; Venrick 1974), the NPSG is now known to harbor the unicellular cyanobacterial groups UCYN-A, UCYN-B (*Crocospheera*) and UCYN-C (*Cyanothece*-like organisms), as well as diverse noncyanobacterial diazotrophs (Zehr et al. 1998; Church et al. 2005a; Farnelid et al. 2011). However, most of our understanding of N_2 fixation in the NPSG comes from studies at Sta. ALOHA (Karl and Church 2014), and less is known

about the spatial variability of diazotrophic communities and NFRs within the broader gyre (although see Church et al. 2008; Moore et al. 2009; Shiozaki et al. 2010, 2017; Villareal et al. 2012). In our study, UCYN-A dominated the *nifH* gene and transcript sequences recovered from all surface NPSG samples. While UCYN-A is present year-round and throughout the euphotic zone at Sta. ALOHA (Church et al. 2009), our study adds to mounting evidence suggesting that this organism may dominate diazotrophic communities in the NPSG during springtime (Church et al. 2009; Böttjer et al. 2014; Gradoville et al. 2017).

A challenge of oceanographic surveys is the attribution of a community process, such as N_2 fixation, to specific organisms. The strong, positive correlation between UCYN-A *nifH* gene abundances and community NFRs during both cruises (Figs. 5, 6) and the absence of such strong relationships for other diazotrophic groups (Table 2) suggest that UCYN-A was the primary diazotroph driving the observed community NFRs in the NPSG. A similar relationship between UCYN-A abundance and hydrogen production (a proxy for N_2 fixation) has been described in the tropical North Atlantic (Moore et al. 2018), suggesting a major contribution of UCYN-A to community N_2 fixation in that region. Additionally, during the 2017 cruise, we directly measured cell-specific NFRs of UCYN-A symbioses in five NPSG stations (Fig. 7). The small differences in cell-specific rates among stations and the absence of a relationship between cell-specific rates and community NFRs suggest that the variability in community NFRs in the NPSG was likely driven by differences in cell abundance rather than by differences in cell-specific activity.

We combined our measurements of UCYN-A cell-specific NFRs with qPCR-derived UCYN-A *nifH* gene abundances to estimate that the bulk contributions of UCYN-A to community NFRs ranged from 9 ± 2 to $40 \pm 18\%$ (Supporting Information - Table S5). This approach has many potential sources of error, including the potential for qPCR *nifH* gene abundances to underestimate or overestimate cell concentrations due to low DNA extraction efficiency (Boström et al. 2004) or polyploidy (Sargent et al. 2016). Furthermore, measuring the ^{15}N enrichment of UCYN-A symbioses after 24 h does not account for the transfer of recently fixed N to other organisms, and the CARD-FISH protocol has been shown to dilute the heavy isotope signal within single cells (Musat et al. 2014), constituting two other potential sources of underestimation relative to community NFR measurements. Although the bulk contribution estimates should be viewed with caution, these estimates support the notion that UCYN-A contributed to community N_2 fixation in the NPSG. Large estimated contributions of UCYN-A to community N_2 fixation have also been reported in the North Atlantic Ocean and the Arctic Ocean (Martinez-Perez et al. 2016; Harding et al. 2018), further supporting the emerging global importance of UCYN-A to marine N_2 fixation.

The large potential contribution of UCYN-A to community NFRs in the NPSG points to a need for understanding the environmental controls of UCYN-A in this region. During

2017, UCYN-A *nifH* gene concentrations within the NPSG varied by a factor of ~13, but the mechanisms driving this observed spatial and/or temporal variability are unclear. UCYN-A abundance within the gyre did not correlate with environmental parameters expected to affect intrinsic growth, such as temperature and the concentrations of iron and macronutrients (Supporting Information Table S4). Thus, our findings may indicate that the differences in UCYN-A abundance among NPSG stations were driven primarily by top-down rather than bottom-up processes. There is evidence that top-down processes may play an important role in controlling UCYN-A abundance: UCYN-A *nifH* gene sequences have been observed in the guts of copepods (Scavotto et al. 2015), and dilution experiments in the NPSG indicate that UCYN-A are preferentially grazed over other diazotrophic taxa (Turk-Kubo et al. 2018). More work is needed in order to understand the environmental controls of UCYN-A and to validate the importance of top-down processes in controlling abundances of this globally abundant marine diazotroph.

Conclusions

We observed clear biogeographical patterns for diazotrophs in the North Pacific. Some diazotrophic groups, including most diazotrophic cyanobacteria, were restricted to the NPSG, while the geographical ranges of noncyanobacterial diazotrophs and of the cyanobacterium UCYN-A extended into the subarctic frontal zone. Our work demonstrates the importance of UCYN-A to N_2 fixation in the NPSG, where UCYN-A abundance correlated strongly with community NFR, while cell-specific NFRs by UCYN-A were more uniform. It is less clear which organisms drive N_2 fixation in the NPTZ, and whether bottom-up (e.g., nutrient supply ratios) or top-down processes are responsible for the sharp shift in diazotrophic abundances and rates observed between the two regimes. This study and others like it demonstrate the need for a better understanding of the ecological controls of uncultivated marine diazotrophs such as UCYN-A.

References

- Ayers, J. M., and M. S. Lozier. 2010. Physical controls on the seasonal migration of the North Pacific transition zone chlorophyll front. *J. Geophys. Res. Oceans* **115**: C05001. doi:10.1029/2009JC005596
- Benavides, M., and others. 2018. Aphotic N_2 fixation along an oligotrophic to ultraoligotrophic transect in the Western Tropical South Pacific Ocean. *Biogeosciences* **15**: 3107–3119.
- Bentzon-Tilia, M., and others. 2015. Significant N_2 fixation by heterotrophs, photoheterotrophs, and heterocystous cyanobacteria in two temperate estuaries. *ISME J.* **9**: 273–285.
- Blais, M., and others. 2012. Nitrogen fixation and identification of potential diazotrophs in the Canadian Arctic. *Global Biogeochem. Cycles* **26**: GB3022.
- Boström, K. H., K. Simu, Å. Hagström, and L. Riemann. 2004. Optimization of DNA extraction for quantitative marine bacterioplankton community analysis. *Limnol. Oceanogr. Methods* **2**: 365–373.
- Böttjer, D., D. M. Karl, R. M. Letelier, D. A. Viviani, and M. J. Church. 2014. Experimental assessment of diazotroph responses to elevated seawater pCO_2 in the North Pacific Subtropical Gyre. *Global Biogeochem. Cycles* **28**: 601–616.
- Böttjer, D., and others. 2017. Temporal variability of nitrogen fixation and particulate nitrogen export at Station ALOHA. *Limnol. Oceanogr.* **62**: 200–216.
- Breitbarth, E., A. Oschlies, and J. LaRoche. 2007. Physiological constraints on the global distribution of *Trichodesmium*: Effect of temperature on diazotrophy. *Biogeosciences* **4**: 53–61.
- Bruland, K. W., E. L. Rue, G. J. Smith, and G. R. DiTullio. 2005. Iron, macronutrients and diatom blooms in the Peru upwelling regime: Brown and blue waters of Peru. *Mar. Chem.* **93**: 81–103.
- Cabello, A. M., and others. 2016. Global distribution and vertical patterns of a prymnesiophyte–cyanobacteria obligate symbiosis. *ISME J.* **10**: 693–706.
- Caporaso, J. G., and others. 2010. QIIME allows analysis of high-throughput community sequencing data. *Nature Methods* **7**: 335–336.
- Chang, B. X., and others. 2019. Low rates of dinitrogen fixation in the eastern tropical South Pacific. *Limnol. Oceanogr.* **64**: 1913–1923.
- Cheung, S., K. Suzuki, X. Xia, and H. Liu. 2019. Transportation of diazotroph community from the upstream to the downstream of the Kuroshio. *J. Geophys. Res. Biogeo.* **124**: 2680–2693.
- Church, M. J., B. D. Jenkins, D. M. Karl, and J. P. Zehr. 2005a. Vertical distributions of nitrogen-fixing phylotypes at Stn ALOHA in the oligotrophic North Pacific Ocean. *Aquat. Microb. Ecol.* **38**: 3–14.
- Church, M. J., C. M. Short, B. D. Jenkins, D. M. Karl, and J. P. Zehr. 2005b. Temporal patterns of nitrogenase gene (*nifH*) expression in the oligotrophic North Pacific Ocean. *Appl. Environ. Microbiol.* **71**: 5362–5370.
- Church, M. J., K. M. Björkman, D. M. Karl, M. A. Saito, and J. P. Zehr. 2008. Regional distributions of nitrogen-fixing bacteria in the Pacific Ocean. *Limnol. Oceanogr.* **53**: 63–77.
- Church, M. J., C. Mahaffey, R. M. Letelier, R. Lukas, J. P. Zehr, and D. M. Karl. 2009. Physical forcing of nitrogen fixation and diazotroph community structure in the North Pacific subtropical gyre. *Global Biogeochem. Cycles* **23**: GB2020.
- Cornejo-Castillo, F. M. 2017. Diversity, ecology and evolution of marine diazotrophic microorganisms. Doctoral dissertation. Polytechnic Univ. of Catalonia.
- Cornejo-Castillo, F. M., and others. 2016. Cyanobacterial symbionts diverged in the late Cretaceous towards lineage-specific nitrogen fixation factories in single-celled phytoplankton. *Nat. Commun.* **7**: 11071.

- Dekas, A. E., and V. J. Orphan. 2011. Identification of diazotrophic microorganisms in marine sediment via fluorescence in situ hybridization coupled to nanoscale secondary ion mass spectrometry (FISH-NanoSIMS), p. 281–305. In M. G. Klotz [ed.], *Methods in enzymology*, v. **486**. Elsevier.
- Delmont, T. O., and others. 2018. Nitrogen-fixing populations of Planctomycetes and Proteobacteria are abundant in surface ocean metagenomes. *Nat. Microbiol.* **3**: 804.
- Deutsch, C., J. L. Sarmiento, D. M. Sigman, N. Gruber, and J. P. Dunne. 2007. Spatial coupling of nitrogen inputs and losses in the ocean. *Nature* **445**: 163–167.
- Díez, B., B. Bergman, C. Pedrós-Alió, M. Antó, and P. Snoeijs. 2012. High cyanobacterial *nifH* gene diversity in Arctic seawater and sea ice brine. *Environ. Microbiol. Rep.* **4**: 360–366.
- Dutkiewicz, S., B. Ward, F. Monteiro, and M. Follows. 2012. Interconnection of nitrogen fixers and iron in the Pacific Ocean: Theory and numerical simulations. *Global Biogeochem. Cycles* **26**: GB1012.
- Edgar, R. C. 2010. Search and clustering orders of magnitude faster than BLAST. *Bioinformatics* **26**: 2460–2461.
- Falkowski, P. G. 1983. Enzymology of nitrogen assimilation, p. 839–868. In E. J. Carpenter and D. G. Capone [eds.], *Nitrogen in the marine environment*. Elsevier.
- Farnelid, H., and others. 2011. Nitrogenase gene amplicons from global marine surface waters are dominated by genes of non-cyanobacteria. *PLoS One* **6**: e19223.
- Ferrón, S., D. A. del Valle, K. M. Björkman, P. D. Quay, M. J. Church, and D. M. Karl. 2016. Application of membrane inlet mass spectrometry to measure aquatic gross primary production by the ^{18}O in vitro method. *Limnol. Oceanogr. Methods* **14**: 610–622.
- Foreman, R. K., M. Segura-Noguera, and D. M. Karl. 2016. Validation of Ti(III) as a reducing agent in the chemiluminescent determination of nitrate and nitrite in seawater. *Mar. Chem.* **186**: 83–89. doi:[10.1016/j.marchem.2016.08.003](https://doi.org/10.1016/j.marchem.2016.08.003)
- Foreman, R. K., K. M. Björkman, C. A. Carlson, K. Opalk, and D. M. Karl. 2019. Improved ultraviolet photo-oxidation system yields estimates for deep-sea dissolved organic nitrogen and phosphorus. *Limnol. Oceanogr. Methods* **17**: 277–291. doi:[10.1002/lom3.10312](https://doi.org/10.1002/lom3.10312)
- Foster, R., A. Subramaniam, C. Mahaffey, E. Carpenter, D. Capone, and J. Zehr. 2007. Influence of the Amazon River plume on distributions of free-living and symbiotic cyanobacteria in the western tropical North Atlantic Ocean. *Limnol. Oceanogr.* **52**: 517–532.
- Galloway, J. N., and others. 2004. Nitrogen cycles: past, present, and future. *Biogeochemistry* **70**: 153–226.
- Goebel, N. L., and others. 2010. Abundance and distribution of major groups of diazotrophic cyanobacteria and their potential contribution to N_2 fixation in the tropical Atlantic Ocean. *Environ. Microbiol.* **12**: 3272–3289.
- Gradoville, M. R., D. Bombar, B. C. Crump, R. M. Letelier, J. P. Zehr, and A. E. White. 2017. Diversity and activity of nitrogen-fixing communities across ocean basins. *Limnol. Oceanogr.* **62**: 1895–1909.
- Gradoville, M. R., B. C. Crump, C. C. Häse, and A. E. White. 2018. Environmental controls of oyster-pathogenic *Vibrio* spp. in Oregon estuaries and a shellfish hatchery. *Appl. Environ. Microbiol.* **84**: e02156–e02117.
- Gruber, N., and J. L. Sarmiento. 1997. Global patterns of marine nitrogen fixation and denitrification. *Global Biogeochem. Cycles* **11**: 235–266.
- Halm, H., and others. 2011. Heterotrophic organisms dominate nitrogen fixation in the South Pacific Gyre. *ISME J.* **6**: 1238–1249.
- Hama, T., T. Miyazaki, Y. Ogawa, T. Iwakuma, M. Takahashi, A. Otsuki, and S. Ichimura. 1983. Measurement of photosynthetic production of a marine phytoplankton population using a stable ^{13}C isotope. *Mar. Biol.* **73**: 31–36.
- Harding, K., K. A. Turk-Kubo, R. E. Sipler, M. M. Mills, D. A. Bronk, and J. P. Zehr. 2018. Symbiotic unicellular cyanobacteria fix nitrogen in the Arctic Ocean. *Proc. Natl. Acad. Sci. U.S.A.* **115**: 13371–13375.
- Hewson, I., and others. 2007. Characteristics of diazotrophs in surface to abyssopelagic waters of the Sargasso Sea. *Aquat. Microb. Ecol.* **46**: 15–30.
- Hu, D., and others. 2015. Pacific western boundary currents and their roles in climate. *Nature* **522**: 299.
- Jayakumar, A., B. X. Chang, B. Widner, P. Bernhardt, M. R. Mulholland, and B. B. Ward. 2017. Biological nitrogen fixation in the oxygen-minimum region of the eastern tropical North Pacific Ocean. *ISME J.* **11**: 2356–2367.
- Juranek, L., P. Quay, R. Feely, D. Lockwood, D. Karl, and M. Church. 2012. Biological production in the NE Pacific and its influence on air-sea CO_2 flux: Evidence from dissolved oxygen isotopes and O_2/Ar . *J. Geophys. Res. Oceans* **117**: C05022.
- Kark, S. 2007. Effects of ecotones on biodiversity. In S. Levin [ed.], *Encyclopedia of biodiversity*. Elsevier.
- Karl, D., R. Letelier, L. Tupas, J. Dore, J. Christian, and D. Hebel. 1997. The role of nitrogen fixation in biogeochemical cycling in the subtropical North Pacific Ocean. *Nature* **388**: 533–538.
- Karl, D., and others. 2002. Dinitrogen fixation in the world's oceans. *Biogeochemistry* **57**: 47–98.
- Karl, D. M., M. J. Church, J. E. Dore, R. M. Letelier, and C. Mahaffey. 2012. Predictable and efficient carbon sequestration in the North Pacific Ocean supported by symbiotic nitrogen fixation. *Proc. Natl. Acad. Sci. U.S.A.* **109**: 1842–1849.
- Karl, D. M., and M. J. Church. 2014. Microbial oceanography and the Hawaii Ocean Time-series programme. *Nature Rev. Microbiol.* **12**: 699–713.
- Klawonn, I., and others. 2015. Simple approach for the preparation of $^{15}\text{-}^{15}\text{N}_2$ -enriched water for nitrogen fixation assessments: Evaluation, application and recommendations. *Front. Microbiol.* **6**: 769.

- Knapp, A. N. 2012. The sensitivity of marine N₂ fixation to dissolved inorganic nitrogen. *Front. Microbiol.* **3**: 374.
- Krupke, A., and others. 2013. In situ identification and N₂ and C fixation rates of uncultivated cyanobacteria populations. *Syst. Appl. Microbiol.* **36**: 259–271.
- Krupke, A., W. Mohr, J. LaRoche, B. M. Fuchs, R. I. Amann, and M. M. Kuypers. 2015. The effect of nutrients on carbon and nitrogen fixation by the UCYN-A-haptophyte symbiosis. *ISME J.* **9**: 1635–1647.
- Lagerström, M. E., M. P. Field, M. Séguret, L. Fischer, S. Hann, and R. M. Sherrell. 2013. Automated on-line flow-injection ICP-MS determination of trace metals (Mn, Fe, Co, Ni, Cu and Zn) in open ocean seawater: Application to the GEOTRACES program. *Mar. Chem.* **155**: 71–80.
- Langlois, R. J., D. Hümmel, and J. LaRoche. 2008. Abundances and distributions of the dominant *nifH* phylotypes in the Northern Atlantic Ocean. *Appl. Environ. Microbiol.* **74**: 1922–1931.
- Langlois, R., T. Großkopf, M. Mills, S. Takeda, and J. LaRoche. 2015. Widespread distribution and expression of Gamma A (UMB), an uncultured, diazotrophic, γ -proteobacterial *nifH* phylotype. *PLoS One* **10**: e0128912.
- Legendre, P. 1998. Model II regression user's guide, R edition. R Vignette. p. 14.
- Legendre, L., and M. Gosselin. 1997. Estimation of N or C uptake rates by phytoplankton using ¹⁵N or ¹³C: Revisiting the usual computation formulae. *J. Plankton Res.* **19**: 263–271.
- Lipschultz, F., and N. J. P. Owens. 1996. An assessment of nitrogen fixation as a source of nitrogen to the North Atlantic Ocean. *Biogeochemistry* **35**: 261–274.
- Loescher, C. R., and others. 2014. Facets of diazotrophy in the oxygen minimum zone waters off Peru. *ISME J.* **8**: 2180–2192.
- Luo, Y.-W., I. Lima, D. Karl, C. Deutsch, and S. Doney. 2014. Data-based assessment of environmental controls on global marine nitrogen fixation. *Biogeosciences* **11**: 691–708.
- Mague, T., N. Weare, and O. Holm-Hansen. 1974. Nitrogen fixation in the North Pacific Ocean. *Mar. Biol.* **24**: 109–119.
- Martinez-Perez, C., and others. 2016. The small unicellular diazotrophic symbiont, UCYN-A, is a key player in the marine nitrogen cycle. *Nat. Microbiol.* **1**: 16163.
- Marumo, R., and O. Asaoka. 1974. Distribution of pelagic blue-green algae in the North Pacific Ocean. *J. Oceanogr. Soc. Japan* **30**: 77–85.
- McGowan, J. A., and P. M. Williams. 1973. Oceanic habitat differences in the North Pacific. *J. Exp. Mar. Biol. Ecol.* **12**: 187–217.
- Mohr, W., T. Großkopf, D. W. R. Wallace, and J. LaRoche. 2010. Methodological underestimation of oceanic nitrogen fixation rates. *PLoS One* **5**: e12583.
- Moisander, P. H., R. A. Beinart, M. Voss, and J. P. Zehr. 2008. Diversity and abundance of diazotrophic microorganisms in the South China Sea during intermonsoon. *ISME J.* **2**: 954–967.
- Moisander, P. H., and others. 2010. Unicellular cyanobacterial distributions broaden the oceanic N₂ fixation domain. *Science* **327**: 1512–1514.
- Moisander, P. H., M. Benavides, S. Bonnet, I. Berman-Frank, A. E. White, and L. Riemann. 2017. Chasing after non-cyanobacterial nitrogen fixation in marine pelagic environments. *Front. Microbiol.* **8**: 1736.
- Montoya, J. P., M. Voss, P. Kahler, and D. G. Capone. 1996. A simple, high-precision, high-sensitivity tracer assay for N₂ fixation. *Appl. Environ. Microbiol.* **62**: 986–993.
- Moonsamy, P., and others. 2013. High throughput HLA genotyping using 454 sequencing and the Fluidigm access Array™ system for simplified amplicon library preparation. *Tissue Antigens* **81**: 141–149.
- Moore, R., S. Punshon, C. Mahaffey, and D. Karl. 2009. The relationship between dissolved hydrogen and nitrogen fixation in ocean waters. *Deep-Sea Res.* **56**: 1449–1458.
- Moore, R., and others. 2018. On the relationship between hydrogen saturation in the Tropical Atlantic Ocean and nitrogen fixation by the symbiotic diazotroph UCYN-A. *J. Geophys. Res. Oceans* **123**: 2353–2362.
- Mulholland, M., and others. 2012. Rates of dinitrogen fixation and the abundance of diazotrophs in North American coastal waters between Cape Hatteras and Georges Bank. *Limnol. Oceanogr.* **57**: 1067–1083.
- Murphy, J., and J. P. Riley. 1962. A modified single solution method for the determination of phosphate in natural waters. *Anal. Chim. Acta* **27**: 31–36. doi:10.1016/S0003-2670(00)88444-5
- Musat, N., and others. 2014. The effect of FISH and CARD-FISH on the isotopic composition of ¹³C- and ¹⁵N-labeled *Pseudomonas putida* cells measured by nanoSIMS. *Syst. Appl. Microbiol.* **37**: 267–276.
- Ohki, K., J. P. Zehr, P. G. Falkowski, and Y. Fujita. 1991. Regulation of nitrogen-fixation by different nitrogen sources in the marine non-heterocystous cyanobacterium *Trichodesmium* sp. NIBB1067. *Arch. Microbiol.* **156**: 335–337.
- Park, K. 1967. Chemical features of the subarctic boundary near 170°W. *J. Fish. Res. Board Can.* **24**: 899–908.
- Polerecky, L., B. Adam, J. Milucka, N. Musat, T. Vagner, and M. M. Kuypers. 2012. Look@ NanoSIMS—A tool for the analysis of nanoSIMS data in environmental microbiology. *Environ. Microbiol.* **14**: 1009–1023.
- Polovina, J. J., E. Howell, D. R. Kobayashi, and M. P. Seki. 2001. The transition zone chlorophyll front, a dynamic global feature defining migration and forage habitat for marine resources. *Prog. Oceanogr.* **49**: 469–483.
- Polovina, J. J., E. A. Howell, D. R. Kobayashi, and M. P. Seki. 2017. The transition zone chlorophyll front updated: Advances from a decade of research. *Prog. Oceanogr.* **150**: 79–85.
- Rees, A. P., J. A. Gilbert, and B. A. Kelly-Gerreyn. 2009. Nitrogen fixation in the western English Channel (NE Atlantic Ocean). *Mar. Ecol. Prog. Ser.* **374**: 7–12.

- Rivero-Calle, S., C. E. Del Castillo, A. Gnanadesikan, A. Dezfali, B. Zaitchik, and D. G. Johns. 2016. Interdecadal *Trichodesmium* variability in cold North Atlantic waters. *Global Biogeochem. Cycles* **30**: 1620–1638.
- Roden, G. I. 1991. Subarctic-subtropical transition zone of the North Pacific: Large-scale aspects and mesoscale structure. NOAA Tech. Rep. NMFS **105**: 1–38.
- Sargent, E. C., and others. 2016. Evidence for polyploidy in the globally important diazotroph *Trichodesmium*. *FEMS Microbiol. Lett.* **363**: fnw244.
- Scavotto, R. E., C. Dziallas, M. Bentzon-Tilia, L. Riemann, and P. H. Moisan. 2015. Nitrogen-fixing bacteria associated with copepods in coastal waters of the North Atlantic Ocean. *Environ. Microbiol.* **17**: 3754–3765.
- Schloss, P. D., and others. 2009. Introducing mothur: Open-source, platform-independent, community-supported software for describing and comparing microbial communities. *Appl. Environ. Microbiol.* **75**: 7537–7541.
- Shiozaki, T., and others. 2010. New estimation of N₂ fixation in the western and Central Pacific Ocean and its marginal seas. *Global Biogeochem. Cycles* **24**: 4482–4489.
- Shiozaki, T., and others. 2017. Basin scale variability of active diazotrophs and nitrogen fixation in the North Pacific, from the tropics to the subarctic Bering Sea. *Global Biogeochem. Cycles* **31**: 996–1009.
- Shiozaki, T., and others. 2017. Diazotroph community structure and the role of nitrogen fixation in the nitrogen cycle in the Chukchi Sea (western Arctic Ocean). *Limnol. Oceanogr.* **63**: 2191–2205.
- Stal, L. J. 2009. Is the distribution of nitrogen-fixing cyanobacteria in the oceans related to temperature? *Environ. Microbiol.* **11**: 1632–1645.
- Strathmann, R. R. 1967. Estimating the organic carbon content of phytoplankton from cell volume or plasma volume. *Limnol. Oceanogr.* **12**: 411–418.
- Strickland, J. D. H., and T. R. Parsons. 1972. A practical handbook of seawater analysis. *Bull. Fish. Res. Board Canada* **167**: 71–80.
- Swalwell, J. E., F. Ribalet, and E. V. Armbrust. 2011. SeaFlow: A novel underway flow-cytometer for continuous observations of phytoplankton in the ocean. *Limnol. Oceanogr. Methods* **9**: 466–477.
- Tang, W., and others. 2019. Revisiting the distribution of oceanic N₂ fixation and estimating diazotrophic contribution to marine production. *Nat. Comm.* **10**: 831.
- Thompson, A., B. J. Carter, K. Turk-Kubo, F. Malfatti, F. Azam, and J. P. Zehr. 2014. Genetic diversity of the unicellular nitrogen-fixing cyanobacteria UCYN-A and its prymnesiophyte host. *Environ. Microbiol.* **16**: 3238–3249.
- Turk-Kubo, K. A., M. Karamchandani, D. G. Capone, and J. P. Zehr. 2014. The paradox of marine heterotrophic nitrogen fixation: Abundances of heterotrophic diazotrophs do not account for nitrogen fixation rates in the Eastern Tropical South Pacific. *Environ. Microbiol.* **16**: 3095–3114.
- Turk-Kubo, K. A., P. Connell, D. Caron, M. E. Hogan, H. M. Farnelid, and J. P. Zehr. 2018. *In situ* diazotroph population dynamics under different resource ratios in the North Pacific Subtropical Gyre. *Front. Microbiol.* **9**: 1616.
- Venrick, E. 1974. The distribution and significance of *Richelia intracellularis* in the North Pacific Central Gyre. *Limnol. Oceanogr.* **19**: 437–445.
- Villareal, T. A., C. G. Brown, M. A. Brzezinski, J. W. Krause, and C. Wilson. 2012. Summer diatom blooms in the North Pacific subtropical gyre: 2008–2009. *PLoS One* **7**: e33109.
- Wang, W.-L., J. K. Moore, A. C. Martiny, and F. W. Primeau. 2019. Convergent estimates of marine nitrogen fixation. *Nature* **566**: 205–211.
- Ward, B. A., S. Dutkiewicz, C. M. Moore, and M. J. Follows. 2013. Iron, phosphorus, and nitrogen supply ratios define the biogeography of nitrogen fixation. *Limnol. Oceanogr.* **58**: 2059–2075.
- Weber, T., and C. Deutsch. 2014. Local versus basin-scale limitation of marine nitrogen fixation. *Proc. Natl. Acad. Sci. U.S.A.* **111**: 8741–8746.
- White, A. E., and others. 2020. A critical review of the ¹⁵N₂ tracer method to measure diazotrophic production in pelagic ecosystems. *Limnol. Oceanogr. Methods*. In press.
- Wilson, C. 2003. Late summer chlorophyll blooms in the oligotrophic North Pacific Subtropical Gyre. *Geophys. Res. Lett.* **30**: 1942.
- Wilson, S. T., D. Böttjer, M. J. Church, and D. M. Karl. 2012. Comparative assessment of nitrogen fixation methodologies, conducted in the oligotrophic North Pacific Ocean. *Appl. Environ. Microbiol.* **78**: 6516–6523.
- Wilson, C., T. A. Villareal, M. A. Brzezinski, J. W. Krause, and A. Y. Shcherbina. 2013. Chlorophyll bloom development and the subtropical front in the North Pacific. *J. Geophys. Res. Oceans* **118**: 1473–1488.
- Yasuda, I. 2003. Hydrographic structure and variability in the Kuroshio-Oyashio transition area. *J. Oceanogr.* **59**: 389–402.
- Zani, S., M. T. Mellon, J. L. Collier, and J. P. Zehr. 2000. Expression of *nifH* genes in natural microbial assemblages in Lake George, New York, detected by reverse transcriptase PCR. *Appl. Environ. Microbiol.* **66**: 3119–3124.
- Zehr, J. P., and L. A. McReynolds. 1989. Use of degenerate oligonucleotides for amplification of the *nifH* gene from the marine cyanobacterium *Trichodesmium thiebautii*. *Appl. Environ. Microbiol.* **55**: 2522–2526.
- Zehr, J. P., M. T. Mellon, and S. Zani. 1998. New nitrogen-fixing microorganisms detected in oligotrophic oceans by amplification of nitrogenase (*nifH*) genes. *Appl. Environ. Microbiol.* **64**: 3444–3450.
- Zehr, J. P., B. D. Jenkins, S. M. Short, and G. F. Steward. 2003. Nitrogenase gene diversity and microbial community structure: A cross-system comparison. *Environ. Microbiol.* **5**: 539–554.

Zehr, J. P., I. N. Shilova, H. M. Farnelid, M. del Carmen Muñoz-Marín, and K. A. Turk-Kubo. 2016. Unusual marine unicellular symbiosis with the nitrogen-fixing cyanobacterium UCYN-A. *Nat. Microbiol.* **2**: 16214.

Zhang, J., K. Kobert, T. Flouri, and A. Stamatakis. 2014. PEAR: A fast and accurate Illumina Paired-End reAd mergeR. *Bioinformatics* **30**: 614–620.

Acknowledgments

This work was funded by the Simons Foundation (Award #426570SP to EVA, AEW, DMK, and JPZ). We are grateful to the SCOPE-Gradients team; we specifically thank R. Foreman for nutrient analyses, N. Hawco for help with tow-fish sampling, A. Hynes for help with flow cytometry analysis, and K. Watkins-Brandt for technical support at sea. We

additionally thank J. Granger for 2017 MIMS analyses, M. Mills and C. Hitzman for help with nanoSIMS analyses, and the captain and crew of the R/V Marcus G. Langseth and the R/V Kaimikai-O-Kanaloa. Finally, we thank three anonymous reviewers for their valuable comments and suggestions.

Conflict of Interest

None declared.

Submitted 07 April 2019

Revised 05 September 2019

Accepted 07 January 2020

Associate editor: Ilana Berman-Frank